of chronic heart failure. European Society of Cardiology Congress 2012, Munchen Germany, 2012. 8

SANBE A, MARUNOUCHI T, HIROSE M, AOKI S, TADA Y, TANONAKA K, NISHIGORI H, TANOUE A: Enhancement of cardiac histone deacetylase 6 (HDAC6) activity protects against cardiac disease in alpha-B-crystallin arg120gly transgenic mouse. European Society of Cardiology Congress 2012, Munchen Germany, 2012. 8

SANBE A, MARUNOUCHI T, HIROSE M, KOIZUMI E, TANONAKA K, NISHIGORI H, TANOUE A: Nicorandil protects cardiomyocytes against alpha-B-crystallin arg120Gly-induced apoptosis. European Society of Cardiology Congress 2012, Munchen Germany, 2012. 8

Hirose M, Takeishi Y. Mechanism underlying GTP-binding protein aq-induced heart failure and cardiac tachycardia. 第90回日本生理学会大会 東京. 2013. 3

H. 知的財産権の出願・登録状況

該当なし

研究成果の刊行に関する一覧表

雑誌

発表者氏名	論文タイトル名	発表誌名	巻号	ページ	出版年
Minami T, Kuwahara K, Nakagawa Y, Takaoka M, Kinoshita H, Nakao K, Kuwabara Y, Yamada Y, Yamada C, Shibata J, Usami S, Yasuno S, Nishikimi T, Ueshima K, Sata M, Nakano H, Seno T, Kawahito Y, Sobue K, Kimura A, Nagai R, Nakao K.	Reciprocal expression of MRTF-A and myocardin is crucial for pathological vascular remodelling in mice.	The EMBO Journal	31	4428-4440	2012
Tanokashira D, Morita T, Hayashi K, Mayanagi T, Fukumoto K, Kubota Y, Yamashita T, Sobue K.	Glucocorticoid suppresses dendritic spine development mediated by down-regulation of caldesmon expression.	The Journal of Neuroscience	32	14583-14591	2012
Morita T., Mayanagi T. and Sobue K.	Caldesmon regulates axon extension through interaction with Myosin II.	Journal of Biological Chemistry	287	3349-3356	2012
Saura H, Ogasawara K, Suzuki T, Kuroda H, Yamashita T, Kobayashi M, Terasaki K, Ogawa A.	Effect of combination therapy with the angiotensin receptor blocker losartan plus hydrochlorothiazide on brain perfusion in patients with both hypertension and cerebral hemodynamic impairment due to symptomatic chronic major cerebral artery steno-occlusive disease: a SPECT study.	Cerebrovascular Disease	33	354-361	2012

Beppu T, Fujiwara S. Nishimoto H, Koeda A, Narumi S, Mori K, Ogasawara K, Sasaki M.	Fractional anisotropy in the centrum semiovale as a quantitative indicator of cerebral white matter damage in the subacute phase in patients with carbon monoxide poisoning: correlation with the concentration of myelin basic protein in cerebrospinal fluid.	Journal of Neurology	259	1698-1705	2012
Matsuura H. Omama S, Yoshida Y, Fujiwara S, Honda T, Akasaka M. Kamei A, Ogasawara K.	Use of magnetic resonance imaging to identify the edge of a dural tear in an infant with growing skull fracture: a case study.	Child's Nervous System	28	1951-1954	2012
Nanba T, Ogasawara K, Nishimoto H, Fujiwara S, Kuroda H, Sasaki M, Kudo K, Suzuki T, Kobayashi M, Yoshida K, Ogawa A.	Postoperative Cerebral White Matter Damage Associated with Cerebral Hyperperfusion and Cognitive Impairment after Carotid Endarterectomy: A Diffusion Tensor Magnetic Resonance Imaging Study.	Cerebrovascular Diseases	34	358-367	2012
Shibui S, Narita Y, Mizusawa J, Beppu T, Ogasawara K, Sawamura Y, Kobayashi H, Nishikawa R, Mishima K, Muragaki Y, Maruyama T, Kuratsu J, Nakamura H, Kochi M, Minamida Y, Yamaki T, Kumabe T, Tominaga H, Kayama T, Sakurada K, Nagase M, Kobayashi K, Nakamura H, Ito T, Yazaki T, Sasaki H, Tanaka K, Takahashi H, Asai A, Todo T, Wakabayashi T, Takahashi J, Takano S. Fujimaki T. Sumi M. Miyakita Y, Nakazato Y. Sato A, Fukuda H, Nomura K.	Randomized trial of chemoradiotherapy and adjuvant chemotherapy with nimustine (ACNU) versus nimustine plus procarbazine for newly diagnosed anaplastic astrocytoma and glioblastoma (JCOG0305).	Cancer Chemotherapy and Pharmacology	71	511-521	2013

Takechi M, Yan J, Hitomi J.	Rare coronary anastomoses between the aorta, pulmonary trunk, left coronary artery, and subclavian artery.	Clinical Anatomy	25	969-972	2012
Saito A, Sasaki M, Ogasawara K, Kobayashi M, Hitomi J, Narumi S, Ohba H, Yamaguchi M, Kudo K, Terayama Y.	Carotid plaque signal differences among four kinds of T1-weighted magnetic resonance imaging techniques: a histopathological correlation study.	Neuroradiology	54	1187-1194	2012
Oikawa M, Saino T, Kimura K, Kamada Y, Tamagawa Y, Kurosaka D, Satoh Y-I.	Effects of protease-activated receptors (PARs) on intracellular calcium dynamics of acinar cells in rat lacrimal glands.	Histochemical Cell Biology		in press	2013
Hirose M, Takeishi Y, Nakada T, Shimojo H, Kashihara T, Nishio A, Suzuki S, Mende U, Matsumoto K, Matsushita N, Taira E, Yamada M.	Nicorandil prevents $G \cdot_{q}$-induced progressive heart failure and ventricular arrhythmias in transgenic mice.	PLOS One.	7	e52667	2012
Hirose M, Matsushita N.	A new therapeutic approach for postoperative systemic inflammation: Effectiveness of epicardial ganglionated plexus stimulation.	Heart Rhythm	9	951-952	2012
Kashihara T, Nakada T, Shimojo H, Horiuchi-Hirose M, Gomi S, Shibazaki T, Sheng X, Hirose M, Hongo M, Yamada M.	Chronic receptor-mediated activation of Gi/o proteins alters basal t-tubular and sarcolemmal L-type Ca2+ channel activity through phosphatases in heart failure.	American Journal of Physiology Heart Circulatory Physiology	302	H1645-H1654	2012
Sheng X, Nakada T, Kobayashi M, Kashihara T, Shibazaki T, Horiuchi-Hirose M, Gomi S, Hirose M, Aoyama T, Yamada M.	Two mechanistically distinct effects of dihydropyridine nifedipine on Ca(V)1.2 L-type Ca(2+) channels revealed by Timothy syndrome mutation.	European Journal of Pharmacology	685	15-23	2012

The EMBO Journal (2012) 31, 4428–4440 | © 2012 European Molecular Biology Organization | All Rights Reserved 0261-4189/12
www.embojournal.org

THE EMBO JOURNAL

Reciprocal expression of MRTF-A and myocardin is crucial for pathological vascular remodelling in mice

Takeya Minami[1], Koichiro Kuwahara[1,*], Yasuaki Nakagawa[1], Minoru Takaoka[2], Hideyuki Kinoshita[1], Kazuhiro Nakao[1], Yoshihiro Kuwabara[1], Yuko Yamada[1], Chinatsu Yamada[1], Junko Shibata[1], Satoru Usami[1], Shinji Yasuno[3], Toshio Nishikimi[1], Kenji Ueshima[3], Masataka Sata[4], Hiroyasu Nakano[5], Takahiro Seno[6], Yutaka Kawahito[6], Kenji Sobue[7], Akinori Kimura[8], Ryozo Nagai[2] and Kazuwa Nakao[1]

[1]Department of Medicine and Clinical Science, Kyoto University Graduate School of Medicine, Kyoto, Japan, [2]Department of Cardiovascular Medicine, Graduate School of Medicine, The University of Tokyo, Tokyo, Japan, [3]EBM Research Center, Kyoto University Graduate School of Medicine, Kyoto, Japan, [4]Department of Cardiovascular Medicine, Institute of Health Biosciences, The University of Tokushima Graduate School, Tokushima, Japan, [5]Laboratory of Molecular and Biochemical Research, Department of Immunology, Biomedical Research Center, Juntendo University Graduate School of Medicine, Tokyo, Japan, [6]Department of Inflammation and Immunology, Graduate School of Medical Science, Kyoto Prefectural University of Medicine, Kyoto, Japan, [7]Department of Neuroscience, Institute for Biomedical Sciences, Iwate Medical University, Iwate, Japan and [8]Department of Molecular Pathogenesis, Medical Research Institute, Tokyo Medical and Dental University, Tokyo, Japan

Myocardin-related transcription factor (MRTF)-A is a Rho signalling-responsive co-activator of serum response factor (SRF). Here, we show that induction of MRTF-A expression is key to pathological vascular remodelling. MRTF-A expression was significantly higher in the wire-injured femoral arteries of wild-type mice and in the atherosclerotic aortic tissues of ApoE$^{-/-}$ mice than in healthy control tissues, whereas myocardin expression was significantly lower. Both neointima formation in wire-injured femoral arteries in MRTF-A knockout (*Mkl1*$^{-/-}$) mice and atherosclerotic lesions in *Mkl1*$^{-/-}$; *ApoE*$^{-/-}$ mice were significantly attenuated. Expression of vinculin, matrix metallopeptidase 9 (MMP-9) and integrin β1, three SRF targets and key regulators of cell migration, in injured arteries was significantly weaker in *Mkl1*$^{-/-}$ mice than in wild-type mice. In cultured vascular smooth muscle cells (VSMCs), knocking down MRTF-A reduced expression of these genes and significantly impaired cell migration. Underlying the increased MRTF-A expression in dedifferentiated VSMCs was the downregulation of microRNA-1. Moreover, the MRTF-A inhibitor CCG1423 significantly reduced neointima formation following wire injury in mice. MRTF-A could thus be a novel therapeutic target for the treatment of vascular diseases.

The EMBO Journal (2012) **31,** 4428–4440. doi:10.1038/emboj.2012.296; Published online 26 October 2012
Subject Categories: molecular biology of disease
Keywords: atherosclerosis; muscle, smooth; remodelling; signal transduction

Introduction

It is now recognized that modulation of vascular smooth muscle cell (VSMC) phenotypes plays a key role in the progression of several prominent cardiovascular disease states, including atherosclerosis, hypertension and restenosis (Schwartz *et al*, 1995; Owens *et al*, 2004). Pathological stress induces a switch from a differentiated VSMC phenotype, characterized by strong expression of contractile proteins and little capacity for migration or proliferation, to a proliferative dedifferentiated phenotype, characterized by relatively weak expression of contractile proteins and an increased capacity for migration and proliferation (Watanabe *et al*, 1999; Owens *et al*, 2004; Nishimura *et al*, 2006). VSMC proliferation and migration contribute to vascular remodelling and obstructive vasculopathies such as atherosclerosis and restenosis following percutaneous coronary intervention (Schwartz *et al*, 1995; Bentzon *et al*, 2006). Cytokines and growth factors locally secreted from cells within the vessel and infiltrating inflammatory cells induce migratory and proliferative responses in VSMCs during vascular remodelling (Owens *et al*, 2004), but the intracellular signalling pathways and the transcriptional regulators of phenotypic modulation of VSMCs are incompletely understood.

Myocardin, myocardin-related transcription factor (MRTF)-A (Mkl1, Bsac or Mal) and MRTF-B (Mkl2) are transcriptional cofactors that associate with serum response factor (SRF), an MADS box transcription factor and critical modulator of cardiovascular differentiation and growth, promoting transcription of a subset of genes involved in cytoskeletal organization and muscle differentiation (Wang *et al*, 2001, 2002; Miano, 2003; Olson and Nordheim, 2010). Myocardin, which is highly restricted to smooth and cardiac muscle cell lineages, is located constitutively in the nucleus and strongly activates transcription of SRF-regulated genes, thereby playing an important role in the differentiation and maintenance of cardiac and smooth muscle cell lineage. By contrast, MRTF-A and -B are expressed more ubiquitously and are found in both the cytoplasm and nucleus. In serum-starved fibroblasts, MRTF-A and -B are localized mainly in the cytoplasm and are translocated into the nucleus in response to stimulation with serum or other

*Corresponding author. Department of Medicine and Clinical Science, Kyoto University Graduate School of Medicine, 54 Shogoin Kawaharacho, Sakyo-ku, Kyoto 606-8507, Japan. Tel.: +81 75 751 4287; Fax: +81 75 771 9452; E-mail: kuwa@kuhp.kyoto-u.ac.jp

Received: 13 May 2012; accepted: 2 October 2012; published online: 26 October 2012

stimuli that promote Rho family GTPase activation and subsequent actin polymerization (Kuwahara *et al*, 2005; Nakamura *et al*, 2010; Olson and Nordheim, 2010). Thus, MRTF-A and -B transduce Rho family GTPase-actin signalling from the cytoplasm to SRF in the nucleus (Miralles *et al*, 2003).

Myocardin knockout leads to death *in utero* due to defects in vascular development (Li *et al*, 2003). In addition, myocardin mRNA levels have been shown to be downregulated in dedifferentiated VSMCs during vascular diseases (Liu *et al*, 2005; Chen *et al*, 2011). In contrast to myocardin, the roles played by MRTF-A in VSMC differentiation and phenotypic modulation remain unclear, though a recent human genetic analysis detected an association between coronary artery disease (CAD) and a single-nucleotide polymorphism (SNP) in the promoter region of the MRTF-A gene that enhances the gene expression (Hinohara *et al*, 2009). Li *et al* (2006) reported that MRTF-A knockout mice were born in anticipated Mendelian ratios, whereas Sun *et al* (2006) reported that MRTF-A knockout mice were born at less than the anticipated Mendelian ratio, which they attributed to fetal loss due to heart failure. In both groups, however, live born MRTF-A knockout pups showed no obvious gross abnormality or cardiovascular defect under normal conditions, except for a defect in maternal lactation due to impaired phenotypic modulation of mammary gland myoepithelial cells (Li *et al*, 2006; Sun *et al*, 2006).

In the present study, we investigated the potential roles of MRTF-A in the pathological processes underlying vascular proliferative diseases. We found that induction of MRTF-A expression is key to pathological remodelling underlying vascular disorders, as it sustains the SRF activity necessary for dedifferentiated VSMCs to acquire the capacity to migrate in response to extracellular stimuli. Our findings suggest that the reciprocal expression of MRTF-A and myocardin is mediated, at least in part, by microRNA (miR)-1 and contributes to the phenotypic modulation of VSMCs during vascular remodelling. These results point to MRTF-A as a potentially useful therapeutic target for the treatment of vascular diseases.

Results

Increased expression of MRTF-A in femoral arteries after wire injury

To explore the potential role played by MRTF-A during pathological vascular remodelling, we initially compared the expression of myocardin, MRTF-A and MRTF-B mRNA between femoral arteries subjected to wire injury or to a sham operation. As seen previously (Liu *et al*, 2005; Chen *et al*, 2011), levels of myocardin mRNA were significantly downregulated in femoral arteries 2 weeks after wire injury, while levels of MRTF-B mRNA were not significantly affected (Figure 1A). By contrast, expression of MRTF-A mRNA was significantly increased in injured arteries, as compared to sham-operated arteries (Figure 1A). Western blot analysis using specific antibodies for myocardin, MRTF-A and MRTF-B, respectively, clearly showed that the level of myocardin protein was reduced in injured arteries, whereas MRTF-A protein was significantly increased (Figure 1B and C; Supplementary Figure S1A). Immunohistochemical analysis showed that cells positively stained for MRTF-A were located mainly in the neointima of injured arteries (Figure 1D; Supplementary Figure S1B). Moreover, in serial sections stained for α-smooth muscle actin (αSMA) and smooth muscle myosin heavy chain (SM-MHC), most of the cells that positively stained for MRTF-A also positively stained for both αSMA and SM-MHC (Figure 1D). Time-course analysis of MRTF-A and myocardin expression revealed that MRTF-A mRNA levels were significantly increased by 2 weeks after injury, when dedifferentiated neointimal VSMCs expressing a relatively low level of αSMA were increasing (Shoji *et al*, 2004; Daniel *et al*, 2010). By 50 days after injury, when a more differentiated population of VSMCs is restored (Daniel *et al*, 2010), MRTF-A mRNA had declined to levels comparable to those seen on day 0 (Supplementary Figure S1C). By contrast, myocardin mRNA levels declined continuously for 2 weeks after injury, but had recovered by 50 days after injury (Supplementary Figure S1D). These results suggest that MRTF-A expression is upregulated in activated, dedifferentiated VSMCs during vascular remodelling, while myocardin expression is downregulated in these cells.

Attenuated vascular remodelling after wire injury in MRTF-A knockout mice

To further evaluate the function of MRTF-A during vascular remodelling, next we performed wire injury in the femoral arteries of MRTF-A knockout ($Mkl1^{-/-}$) mice. As previously reported, the $Mkl1^{-/-}$ mice were viable, fertile and showed no significant gross abnormalities or cardiovascular defects under normal conditions (Li *et al*, 2006). There was no difference in blood pressure or heart rate between wild-type and $Mkl1^{-/-}$ mice (Figure 2A), and the thickness of the medial wall in the uninjured sham-operated femoral arteries was comparable between wild-type and $Mkl1^{-/-}$ mice (Table I). Femoral arterial expression of myocardin mRNA was significantly weaker in $Mkl1^{-/-}$ mice 2 weeks after wire injury than in sham-operated arteries, just as was observed with wild-type mice (Figure 2B). On the other hand, neointima-to-medial ratios determined 4 weeks after wire injury were significantly smaller in $Mkl1^{-/-}$ mice than in wild-type mice, whereas there was no difference in medial thickness in the injured arteries between wild-type and $Mkl1^{-/-}$ mice (Figure 2C and D; Table I).

Four weeks after wire injury, the neointimal area comprised cells positively stained for αSMA was markedly smaller in $Mkl1^{-/-}$ mice than in wild-type mice (Figure 2D). Immunohistochemical analysis in serial sections stained for SM-MHC showed overlap with αSMA-positive cells (Figure 2D), suggesting that a reduction in the numbers of dedifferentiated VSMCs within the neointima is largely responsible for the reduction in the neointima-to-medial ratios seen in $Mkl1^{-/-}$ mice. Indeed, the numbers of Ki-67-positive proliferating cells within the injured vessels were also significantly lower in $Mkl1^{-/-}$ mice than in wild-type mice (Figure 2E and F). By contrast, the numbers of TUNEL-positive or cleaved caspase-3-positive apoptotic cells within the injured arteries did not differ between wild-type and $Mkl1^{-/-}$ mice (Supplementary Figure S2A through D). Similarly, the % fibrotic area in the media and intima and expression of the genes encoding collagen type 1 alpha1 and collagen type3 alpha1 within the injured arteries also did not significantly differ between wild-type and $Mkl1^{-/-}$ mice

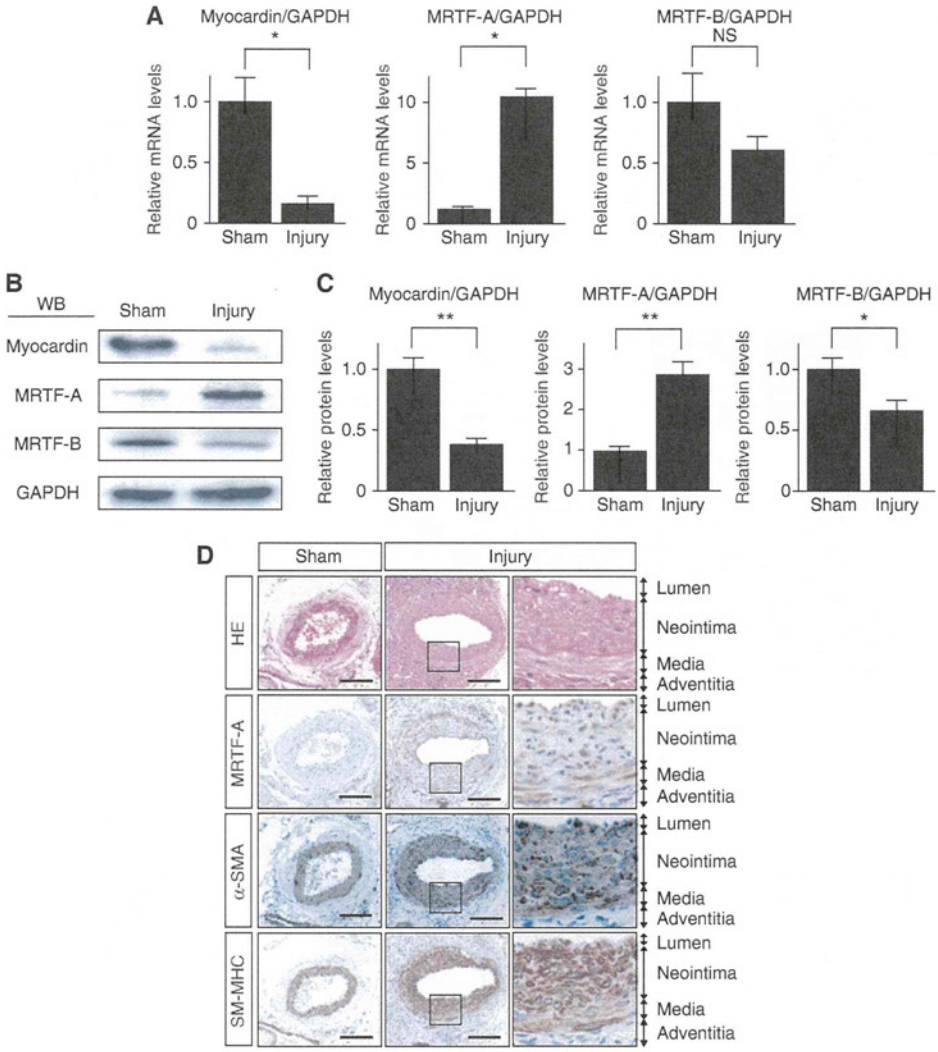

Figure 1 Increased expression of MRTF-A in femoral arteries after wire injury in mice. (**A**) Real-time RT–PCR analysis showing relative levels of myocardin, MRTF-A and MRTF-B mRNAs (normalized to GAPDH mRNA) in femoral arteries 2 weeks after wire injury (injury) ($n=6$ each). The relative mRNA level in sham-operated arteries (sham) was assigned a value of 1.0. (**B**) Representative western blots showing myocardin, MRTF-A and MRTF-B in wire-injured and sham-operated femoral arteries (2 weeks after injury). (**C**) The relative protein levels (normalized to GAPDH) of myocardin, MRTF-A and MRTF-B in wire-injured and sham-operated femoral arteries ($n=4$ each). The relative protein level in the sham-operated arteries was assigned a value of 1.0. (**D**) Immunohistochemical analysis of MRTF-A expression in sham-operated and wire-injured femoral arteries. Tissues are labelled with anti-BSAC (MRTF-A), anti-α-smooth muscle actin (αSMA) or anti-smooth muscle myosin heavy chain (SM-MHC) antibodies; bar indicates 100 μm. Three different experiments gave identical results. All graphs are shown as means ± s.e.m. $*P<0.05$. $**P<0.001$. NS, not significant. Figure source data can be found with the Supplementary data.

(Supplementary Figure S2E through G). In addition, because multiple cell types other than dedifferentiated VSMCs can contribute to neointima formation and to the vascular remodelling process, we also stained the tissue for endothelial cell (CD31) and macrophage (Mac3) markers. The relative numbers of CD31-positive and Mac3-positive cells in the injured arteries did not differ between wild-type and *Mkl1*$^{-/-}$ mice (Figure 2G through I), which indicates that a reduction in the number of αSMA-positive dedifferentiated VSMCs contributes to the attenuation of vascular remodelling in wire-injured *Mkl1*$^{-/-}$ mice. We also examined neointima formation following carotid artery ligation in *Mkl1*$^{-/-}$ mice, and found that neointima formation 4 weeks after carotid ligation was significantly diminished in *Mkl1*$^{-/-}$ mice, as compared to control *Mkl*$^{+/-}$ mice (Supplementary Figure S2H and I; Supplementary Table S1).

Loss of MRTF-A attenuates atherosclerotic lesions in APOE$^{-/-}$ *mice*

We next sought to analyse MRTF-A expression in a model of a different type of vascular disorder. *ApoE*$^{-/-}$ mice are prone to atherosclerotic lesions, to which both dedifferentiated VSMCs and infiltrating inflammatory cells contribute (Glass and Witztum, 2001; Bentzon *et al*, 2006). MRTF-A gene expression was significantly upregulated in aortic tissues containing atherosclerotic lesions in *ApoE*$^{-/-}$ mice fed a high cholesterol diet for 8 weeks (from 8 to 16 weeks of age), as compared to normal wild-type aortic tissues in

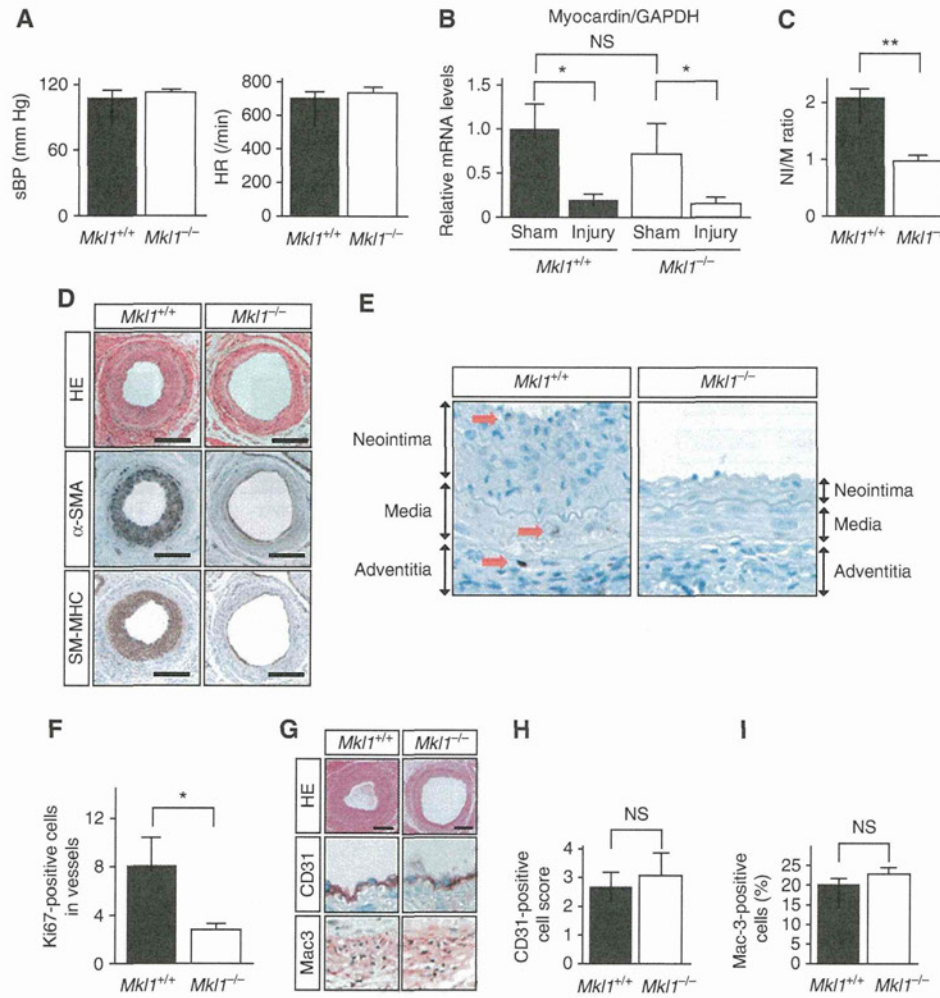

Figure 2 Attenuated vascular remodelling in response to wire injury in *Mkl1*$^{-/-}$ mice. (**A**) Systolic blood pressure (sBP) and heart rate (HR) in control *Mkl1*$^{+/+}$ and *Mkl1*$^{-/-}$ mice ($n=5$ each). (**B**) The relative levels of myocardin mRNA in wire-injured and sham-operated femoral arteries in *Mkl1*$^{+/+}$ and *Mkl1*$^{-/-}$ mice ($n=5$ each). (**C**) The neointima (NI)-to-media (M) ratio in arteries 4 weeks after wire injury in *Mkl1*$^{+/+}$ and *Mkl1*$^{-/-}$ mice ($n=20$ each). (**D**) Representative images of neointima in arteries 4 weeks after wire injury in *Mkl1*$^{+/+}$ and *Mkl1*$^{-/-}$ mice. HE: haematoxylin-eosin staining. α-SMA: staining with anti-α-SMA antibody. SM-MHC: staining with anti-SM-MHC antibody. (**E**) Representative images of neointima 4 weeks after femoral artery injury stained with anti-Ki-67 antigen in *Mkl1*$^{+/-}$ and *Mkl1*$^{-/-}$ mice. Red arrows indicate Ki-67-positive cells. (**F**) Numbers of Ki-67-positive cells in injured vessels of *Mkl1*$^{+/+}$ and *Mkl1*$^{-/-}$ mice 4 weeks after wire injury are shown ($n=3$ in each group). (**G**) Representative images of neointima stained with anti-CD31 (CD31) or anti-Mac3 (Mac3) antibody in arteries from *Mkl1*$^{+/+}$ and *Mkl1*$^{-/-}$ mice 4 weeks after wire injury. (**H**, **I**) The semi-quantitative CD31-positive scores ($n=5$ in each group) (**H**) and the relative numbers of Mac3-positive cells (% positive cells/total cells in neointima and media; $n=4$ in each group) (**I**) in *Mkl1*$^{+/+}$ and *Mkl1*$^{-/-}$ mice 4 weeks after wire injury are shown. All graphs are shown as means ± s.e.m. *$P<0.05$. **$P<0.001$. NS, not significant.

Table I Luminal and neointimal area of femoral arteries 4 weeks after vascular injury

	n	Lumen ($\times 10^3/\mu m^2$)	Intima ($\times 10^3/\mu m^2$)	Media ($\times 10^3/\mu m^2$)	IEL ($\times 10^3/\mu m^2$)	EEL ($\times 10^3/\mu m^2$)	Intima/Media ratio
Mkl1$^{+/+}$ sham	4	11.9 ± 2.7	0	19.0 ± 1.2	11.9 ± 2.7	30.9 ± 3.3	0
Mkl1$^{-/-}$ sham	4	10.4 ± 2.8	0	20.2 ± 2.5	10.4 ± 2.8	30.6 ± 2.8	0
Mkl1$^{+/+}$ injury	20	24.9 ± 3.5	39.7 ± 5.0	18.8 ± 1.1	64.8 ± 4.6	84.0 ± 5.4	2.09 ± 0.17
Mkl1$^{-/-}$ injury	20	29.6 ± 3.9	22.0 ± 2.3*	22.7 ± 1.2	52.3 ± 4.6	75.3 ± 5.3	0.96 ± 0.10*

The ratio of intima to media was calculated as the intimal area/medial area. Values are means ± s.e.m. IEL, internal elastic lamina; EEL, external elastic lamina. *$P<0.01$ versus *Mkl1*$^{+/+}$ injured arteries.

age-matched mice (Figure 3A). By contrast, myocardin gene expression was significantly decreased in atherosclerotic aortas, compared to normal aortas (Figure 3A). Consistent with that finding, cells positively stained for MRTF-A were observed within atherosclerotic lesions in the proximal aorta of *ApoE*$^{-/-}$ mice (Figure 3B).

To evaluate directly the contribution of MRTF-A to the development of atherosclerotic lesions in *ApoE*$^{-/-}$ mice, we crossed *Mkl1*$^{-/-}$ and *Apo E*$^{-/-}$ mice. Although the blood pressures, heart rates, cholesterol profiles and myocardin gene expression in aortic tissues did not differ between *Mkl1*$^{+/+}$;*ApoE*$^{-/-}$ and *Mkl1*$^{-/-}$;*ApoE*$^{-/-}$ mice

(Supplementary Figure S3A; Figure 3C), en-face analysis of the global progression of atherosclerotic lesions throughout the aorta revealed that the aortas of *Mkl1*$^{-/-}$;*ApoE*$^{-/-}$ mice contained smaller atherosclerotic lesions than those of *Mkl1*$^{+/+}$;*ApoE*$^{-/-}$ mice (Figure 3D). Furthermore, cross-sectional analysis of the proximal aorta revealed the average lesion area at the aortic root of *Mkl1*$^{-/-}$;*ApoE*$^{-/-}$ mice (2.5%) to be significantly smaller than at the aortic root of *Mkl1*$^{+/+}$; *ApoE*$^{-/-}$ mice (11.8%, $P<0.05$ versus *Mkl1*$^{-/-}$;*ApoE*$^{-/-}$) (Figure 3E and F). The relative accumulation of macrophages within atherosclerotic lesions at the aortic root, which was estimated based on the size of the

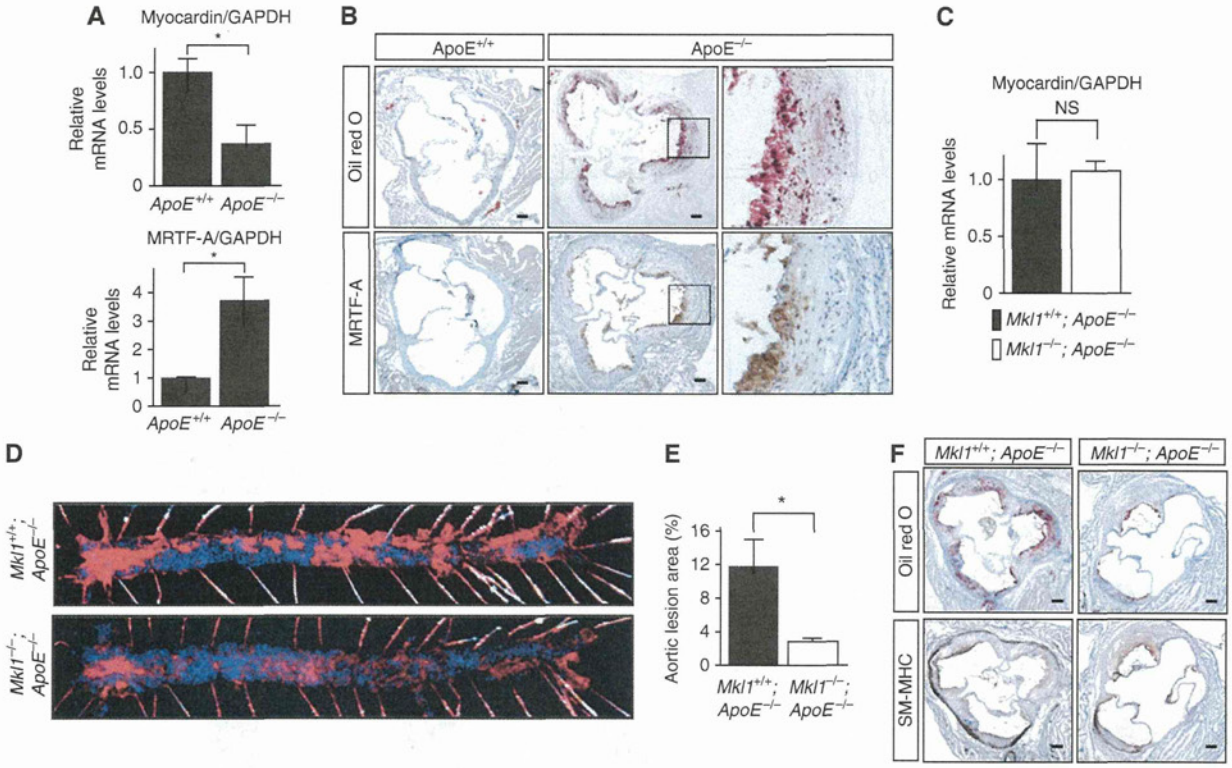

Figure 3 Atherosclerotic lesions in *Mkl1*$^{-/-}$;*ApoE*$^{-/-}$ mice are attenuated, as compared to those in *Mkl1*$^{+/+}$;*ApoE*$^{-/-}$ mice. (**A**) Real-time RT–PCR analysis showing the relative levels of MRTF-A and myocardin mRNAs (normalized to GAPDH mRNA) in atherosclerotic aortas from *ApoE*$^{-/-}$ mice fed a high-cholesterol diet and normal aortas from *ApoE*$^{+/+}$ mice at 16 weeks of age ($n=4$ each). *$P<0.05$. (**B**) Representative images showing MRTF-A expression within an atherosclerotic lesion in the proximal aorta of *ApoE*$^{-/-}$ mice. The tissues from *Apo*$^{+/+}$ and *ApoE*$^{-/-}$ mice were stained using anti-BSAC antibodies (MRTF-A). Oil-red O: Oil-red O staining. Three different experiments gave identical results. (**C**) Real-time RT–PCR analysis showing the relative levels of myocardin mRNA in atherosclerotic aortas from *Mkl1*$^{-/-}$;*ApoE*$^{-/-}$ and *Mkl1*$^{+/+}$;*ApoE*$^{-/-}$ mice fed a high-cholesterol diet ($n=4$ each). (**D**) Representative images of atherosclerotic lesions from an en-face analysis of the total aorta in *Mkl1*$^{+/+}$;*ApoE*$^{-/-}$ and *Mkl1*$^{-/-}$;*ApoE*$^{-/-}$ mice fed a high-cholesterol diet. Sudan III staining. Three independent experiments showed identical results. Red colour shows lipid-laden areas representing atherosclerotic lesions. (**E**) Graphs showing the relative (%) area of atherosclerotic lesions in cross-sections of proximal aorta from *Mkl1*$^{+/+}$;*ApoE*$^{-/-}$ and *Mkl1*$^{-/-}$;*ApoE*$^{-/-}$ mice fed a high-cholesterol diet for 8 weeks ($n=8$ each). *$P<0.05$. (**F**) Representative images of atherosclerotic lesions in cross-sections of proximal aorta from *Mkl1*$^{+/+}$;*ApoE*$^{-/-}$ and *Mkl1A*$^{-/-}$;*ApoE*$^{-/-}$ mice fed a high-cholesterol diet. Oil-red O: Oil-red O staining. SM-MHC: staining with anti-SM-MHC antibody. Bar indicates 100 μm. All graphs are shown as means ± s.e.m.

Figure 4 MRTF-A mediates acquisition of migration capacity by dedifferentiated VSMCs through regulation of SRF-target genes. (**A**) Real-time RT–PCR analysis showing relative levels of vinculin, MMP9 and integrin β1 mRNAs (normalized to GAPDH mRNA) in femoral arteries 2 weeks after wire injury in *Mkl1*$^{+/+}$ and *Mkl1*$^{-/-}$ mice ($n=4$ each). (**B**) Representative western blots showing myocardin, MRTF-A and MRTF-B in arteries 2 weeks after wire injury, in sham-operated arteries and in cultured mouse aortic VSMCs (MAVSMCs) and rat aortic VSMCs (RAVSMCs). (**C**) Real-time RT–PCR analysis showing the relative levels of myocardin, MRTF-A and MRTF-B mRNAs in femoral arteries 2 weeks after wire injury (injury), in sham-operated arteries (sham) and in cultured MAVSMCs and RAVSMCs ($n=6$ each). (**D**) Real-time RT–PCR analysis showing relative levels of MRTF-A, myocardin, vinculin, MMP9 and integrin β1 mRNAs in RAVSMCs transfected with MRTF-A siRNA or control siRNA ($n=6$ each). (**E**) Co-transfection of a plasmid expressing MRTF-A (0, 10 and 100 ng) plus the luciferase reporter gene driven by bp −360 to +63 of the 5′-flanking region of vinculin gene (vinculin-luc) into RAVSMCs (left panel) and NIH3T3 cells (right panel). Relative luciferase activities normalized to Renilla luciferase (pRL-TK) activity are shown. Vinculin CArG-mut-luc: luciferase reporter gene driven by the vinculin promoter harbouring a mutation within the CArG-box. Data were obtained from three experiments performed in sextuplicate. (**F**) Co-transfection of MRTF-A siRNA plus vinculin-luc into RAVSMCs. Relative luciferase activities normalized to Renilla luciferase activity are shown. Data were obtained from two experiments performed in sextuplicate. (**G**) Migration in the presence or absence of PDGF-BB of RAVSMCs transfected with MRTF-A siRNA or control siRNA. Data were obtained from three experiments performed in sextuplicate. (**H**) Proliferation in the presence or absence of fetal calf serum (FCS) of RAVSMCs transfected with MRTF-A siRNA or control siRNA. Data were obtained from three experiments performed in sextuplicate. All graphs are shown as means ± s.e.m. *$P<0.05$ and **$P<0.01$. NS, not significant. Figure source data can be found with the Supplementary data.

F4/80-stained area normalized to the corresponding total atherosclerotic lesion area, did not significantly differ between *Mkl1*$^{+/+}$;*ApoE*$^{-/-}$ and *Mkl1*$^{-/-}$;*ApoE*$^{-/-}$ mice (Supplementary Figure S3B).

MRTF-A is necessary for acquisition of migratory capacity in dedifferentiated VSMCs

SRF controls cellular migration capacity in various cell types, including dedifferentiated VSMCs, by regulating the expres-

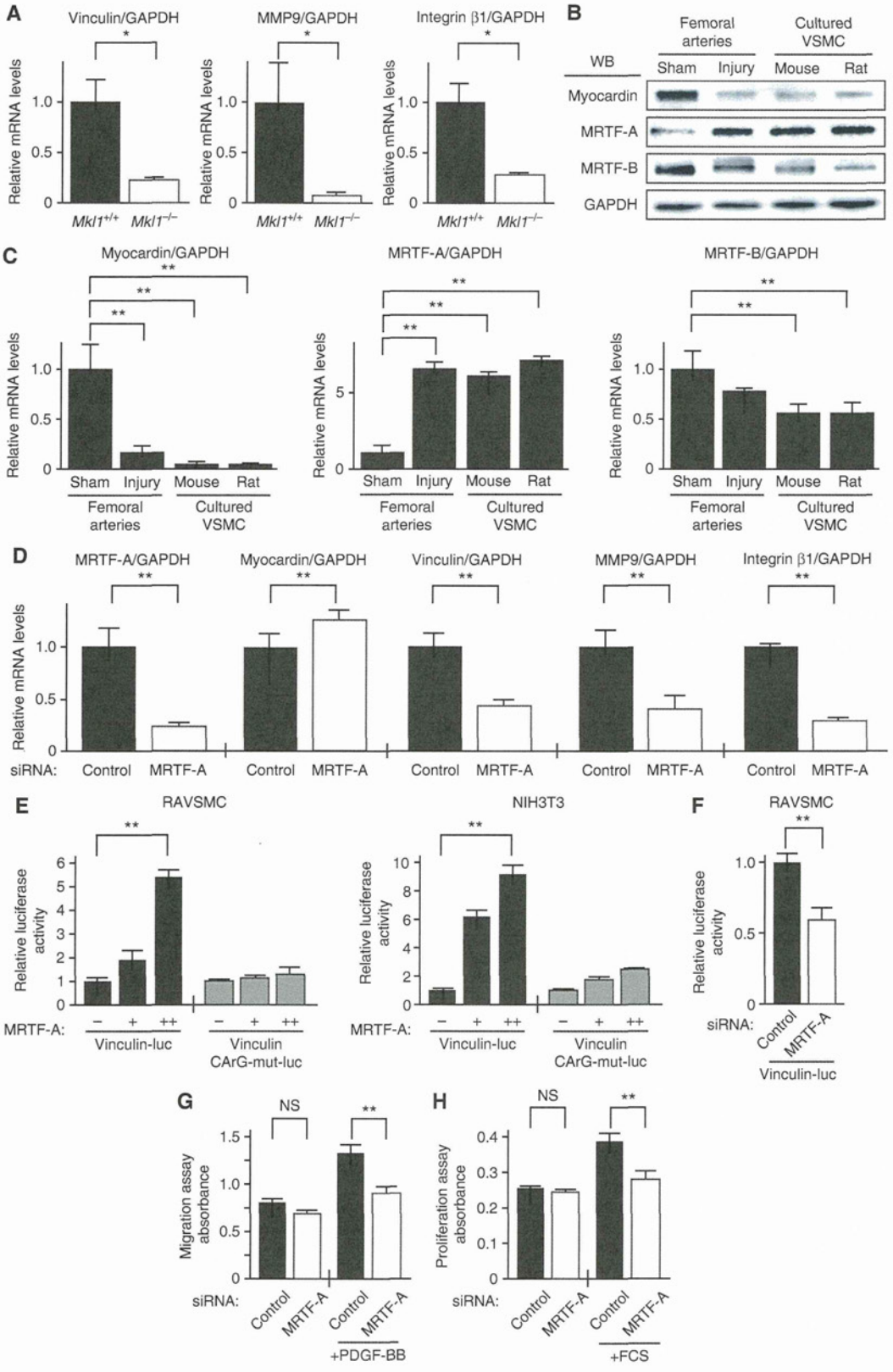

sion of several target genes, including the genes encoding vinculin, MMP9 and integrin β1 (Kenagy *et al*, 1997; Xu *et al*, 1998; Morita *et al*, 2007; Medjkane *et al*, 2009; Olson and Nordheim, 2010). We therefore examined the expression of these SRF-target genes in wire-injured femoral arteries. We found that 2 weeks after wire injury there was significantly less expression of vinculin, MMP9 and integrin β1 genes in the injured femoral arteries of $Mkl1^{-/-}$ mice than control $Mkl1^{+/+}$ mice (Figure 4A). The expression of these genes in the intact femoral arteries of $Mkl1^{-/-}$ and control $Mkl1^{+/+}$ mice was not significantly different (Supplementary Figure S4A). The mRNA expression of other SRF targets, αSMA (*ACTA2*) and SM-MHC (*Myh11*) genes encoding smooth muscle-specific contractile proteins, was also significantly less in the injured femoral arteries of $Mkl1^{-/-}$ mice than $Mkl1^{+/+}$ mice (Supplementary Figure S4B). In primary mouse aortic VSMCs (MAVSMCs), a cellular model of dedifferentiated VSMCs in which MRTF-A expression is increased and myocardin expression is decreased (Figure 4B and C; Supplementary Figure S4C; Hinson *et al*, 2007; Nakamura *et al*, 2010), levels of vinculin, MMP9, integrin β1 and αSMA mRNA were significantly reduced after knocking down MRTF-A (Figure 4D; Supplementary Figure S4D). This suggests that MRTF-A plays a predominant role in maintaining the expression of several SRF-target genes involved in cellular migration in dedifferentiated VSMCs, where expression of myocardin is decreased (Figure 4B and C; Nakamura *et al*, 2010). Overexpression of MRTF-A stimulated vinculin promoter activity in an SRF-dependent manner in both primary rat aortic VSMCs (RAVSMCs) and NIH3T3 fibroblasts (Figure 4E), whereas knocking down MRTF-A reduced vinculin promoter activity in RAVSMCs (Figure 4F). This supports the conclusion that MRTF-A regulates the expression of SRF-target genes in dedifferentiated VSMCs. Furthermore, knocking down MRTF-A significantly impaired PDGF-BB-induced RAVSMC migration, whereas knocking down myocardin did not (Figure 4G; Supplementary Figure S4E and F).

Because SRF is also known to control cellular proliferation, we examined the effect of MRTF-A knockdown on RAVSMC proliferation, and found that knocking down MRTF-A significantly reduced serum-induced RAVSMC proliferation, whereas knocking down myocardin did not (Figure 4H; Supplementary Figure S4G).

Reduced miR-1 expression contributes to the increase in MRTF-A expression in dedifferentiated VSMCs

We next investigated the molecular mechanisms potentially involved in regulating the reciprocal expression of MRTF-A and myocardin during VSMC dedifferentiation. We initially hypothesized that increased expression of myocardin leads to the repression of MRTF-A gene transcription through either direct or indirect mechanisms. Within the MRTF-A gene, the 5′-flanking region (FR) up to 1 kbp from the transcription start site is well conserved among different species. However, we failed to detect any significant effects of myocardin or MRTF-A on the activity of −930 bp MRTF-A promoter region in either RAVSMCs or NIH3T3 cells (Figure 5A; Supplementary Figure S5A). Myocardin also did not significantly affect the promoter activity of −5500 bp MRTF-A promoter region in either RAVSMCs or NIH3T3 cells (Supplementary Figure S5B). We therefore focused on the role of the 3′-untranslated region (UTR) of MRTF-A mRNA, where we found a conserved target site for microRNA-1 (miR-1) (Figure 5B). We observed that expression of miR-1 in vascular tissues is >100 times higher than in several non-muscle tissues, though its expression in skeletal and cardiac muscle tissues is much higher (Figure 5C). Consistent with earlier reports that miR-1 expression is regulated by myocardin and SRF in VSMCs and is downregulated in neointimal lesions created by ligation of carotid arteries of mice (Zhao *et al*, 2005; Chen *et al*, 2011), miR-1 expression was significantly weaker in the injured femoral arteries and atherosclerotic aorta of $ApoE^{-/-}$ mice, where there was a corresponding reduction of myocardin expression, than in control arteries (Figures 1A through C and 5D; Supplementary Figure S5C). Levels of miR-1 expression were also substantially lower in cultured RAVSMCs than in normal arteries (Supplementary Figure S5D). Overexpression of a miR-1 mimic significantly reduced endogenous MRTF-A gene and protein expression in RAVSMCs (Figure 5E and F), whereas overexpression of a miR-1 inhibitor significantly increased MRTF-A mRNA and protein expression (Figure 5G and H).

We also assessed miR-1-induced repression of MRTF-A gene by placing its 3′-UTR downstream of a cytomegalovirus (CMV)-driven luciferase reporter and performing luciferase assays in COS7 cells transfected with a miR-1 mimic or control scrambled oligo (Figure 5I). The miR-1 mimic significantly reduced the activity of the luciferase reporter linked to the MRTF-A 3′-UTR, and a mutation in the predicted miR-1 binding site in the 3′-UTR prevented that repression (Figure 5J). Moreover, overexpression of myocardin in A7r5 VSMCs significantly repressed the activity of a luciferase reporter gene linked to the MRTF-A 3′-UTR in a miR-1-dependent fashion (Figure 5K). These results strongly suggest that reduced expression of miR-1 caused by the reduction in myocardin expression during the process of phenotypic modulation of VSMCs contributes to the increase in MRTF-A expression in dedifferentiated VSMCs. Consistent with those findings, injection of an anti-miR-1 Locked Nucleic Acid (LNA)™-enhanced microRNA inhibitor into the injured vessels led to an increase in MRTF-A gene expression and exacerbated the pathological vascular remodelling after wire injury (Supplementary Figure S5E through G; Supplementary Table S2).

Pharmacological inhibition of MRTF-A activity attenuates adverse vascular remodelling after wire injury

The results presented raise the possibility that MRTF-A is a novel therapeutic target for the treatment of vascular disease. Recently, a small molecule (CCG-1423) was found to inhibit Rho pathway-mediated SRF activation (Evelyn *et al*, 2007; Jin *et al*, 2011). CCG-1423 appears to inhibit the interaction between SRF and MRTF-A at a point upstream of the DNA binding. Although the site of inhibition and its selectivity is not yet precisely defined, it was recently shown that CCG-1423 blocks nuclear translocation of MRTF-A, thereby inhibiting MRTF-A-mediated effects on SRF transcription, at least in part (Jin *et al*, 2011). In addition, we confirmed that CCG-1423 blocks serum-induced nuclear accumulation of endogenous MRTF-A in RAVSMCs (Figure 6A). CCG-1423 also significantly blocked SRF activity induced by co-expres-

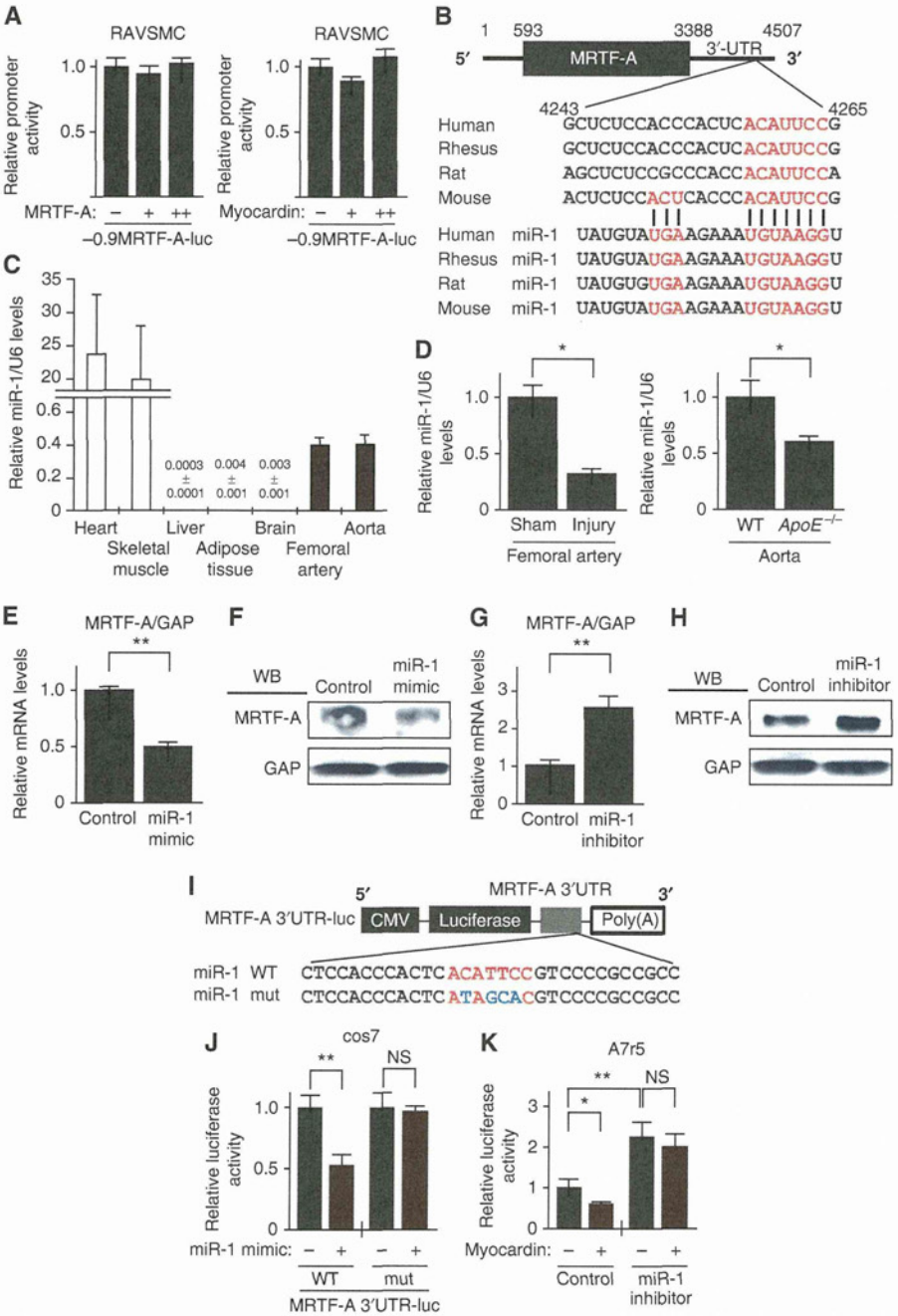

Figure 5 MicroRNA-1 regulates MRTF-A gene expression. (**A**) Co-transfection of a plasmid encoding myocardin or MRTF-A (0, 10 and 100 ng) with the −930 bp MRTF-A-luc gene into RAVSMCs. Data were obtained from two experiments performed in quadruplicate. +: 10 ng. ++: 100 ng. (**B**) Schematic representation of the MRTF-A 3′-untranslated region (UTR) containing a conserved microRNA-1 (miR-1) target site (shown in red). Sequences of mature miR-1 in different species are shown below. (**C**) Real-time RT–PCR analysis showing the relative miR-1 expression (normalized to the U6 levels) in different mouse tissues. (**D**) Real-time RT–PCR analysis showing the relative miR-1 expression (normalized to the U6 levels) in femoral arteries 2 weeks after wire injury or sham operation in wild-type mice ($n=4$ each) (left panel), and in aortic tissues in *ApoE*$^{-/-}$ or control wild-type mice (right panel). (**E**) Endogenous expression of MRTF-A mRNA in RAVSMCs transfected with miR-1 mimic or control oligo. Graphs show the relative MRTF-A mRNA levels (normalized to GAPDH mRNA) ($n=4$ each). (**F**) Representative western blots showing the effect of miR-1 mimic on MRTF-A expression in RAVSMCs. Three different experiments gave identical results. (**G**) Endogenous MRTF-A mRNA expression in RAVSMCs transfected with miR-1 inhibitor. Graphs show the relative MRTF-A mRNA levels ($n=4$ each). (**H**) Representative western blots showing the effect of a miR-1 inhibitor on MRTF-A expression in RAVSMCs. Three different experiments gave identical results. (**I**) Luciferase reporter constructs containing wild-type and mutant MRTF-A 3′UTR (MRTF-A 3′UTR-luc and mutMRTF-A 3′UTR-luc, respectively). The conserved miR-1 target site is shown in red. In mutMRTF-A 3′UTR-luc, mutations were introduced within the miR-1 target site (shown in blue). (**J**) MRTF-A 3′UTR-luc and mutMRTF-A 3′UTR-luc were co-transfected with miR-1 mimic into COS7 cells for 48 h. Data were obtained from three experiments performed in quadruplicate. (**K**) MRTF-A 3′UTR-luc was transfected with or without a plasmid expressing myocardin and/or a miR-1 inhibitor into A7r5 cells for 48 h. Data were obtained from three experiments performed in quadruplicate. All graphs are shown as means ± s.e.m. Relative luciferase activities normalized to control Renilla luciferase activity are shown. *$P<0.05$. **$P<0.01$. NS, not significant. Figure source data can be found with the Supplementary data.

sion of striated muscle activator of rho signalling (STARS) and MRTF-A in RAVSMCs (Figure 6B; Kuwahara *et al*, 2005). STARS is an actin-binding protein that activates SRF by inducing nuclear accumulation of MRTF-A. Both CCG-1423 and MRTF-A knockdown similarly inhibited STARS-induced activation of SRF in RAVSMCs. Furthermore, this inhibitory effect of CCG-1423 on STARS-induced activation of SRF was abolished by knocking down MRTF-A, supporting the notion that CCG-1423 blocks MRTF-A-mediated activation of SRF (Supplementary Figure S6A) Similarly to knocking down MRTF-A, CCG-1423 significantly reduced the migration and proliferation capacities of RAVSMCs (Figure 6C and D). When we then treated mice subjected to femoral artery wire injury with CCG-1423 (0.15 mg/kg intraperitoneally for 3 weeks), we found that CCG-1423 significantly attenuated the progression of vascular remodelling in arteries 3 weeks after injury (Figure 6E and F; Table II; Supplementary Figure S6B and C), without affecting the hemodynamic parameters or cholesterol profiles (Supplementary Figure S6D and E). CCG-1423 did not affect gross appearance, body weight or survival among the mice during the experiment (data not shown). Furthermore, administration of CCG-1423 also significantly attenuated the

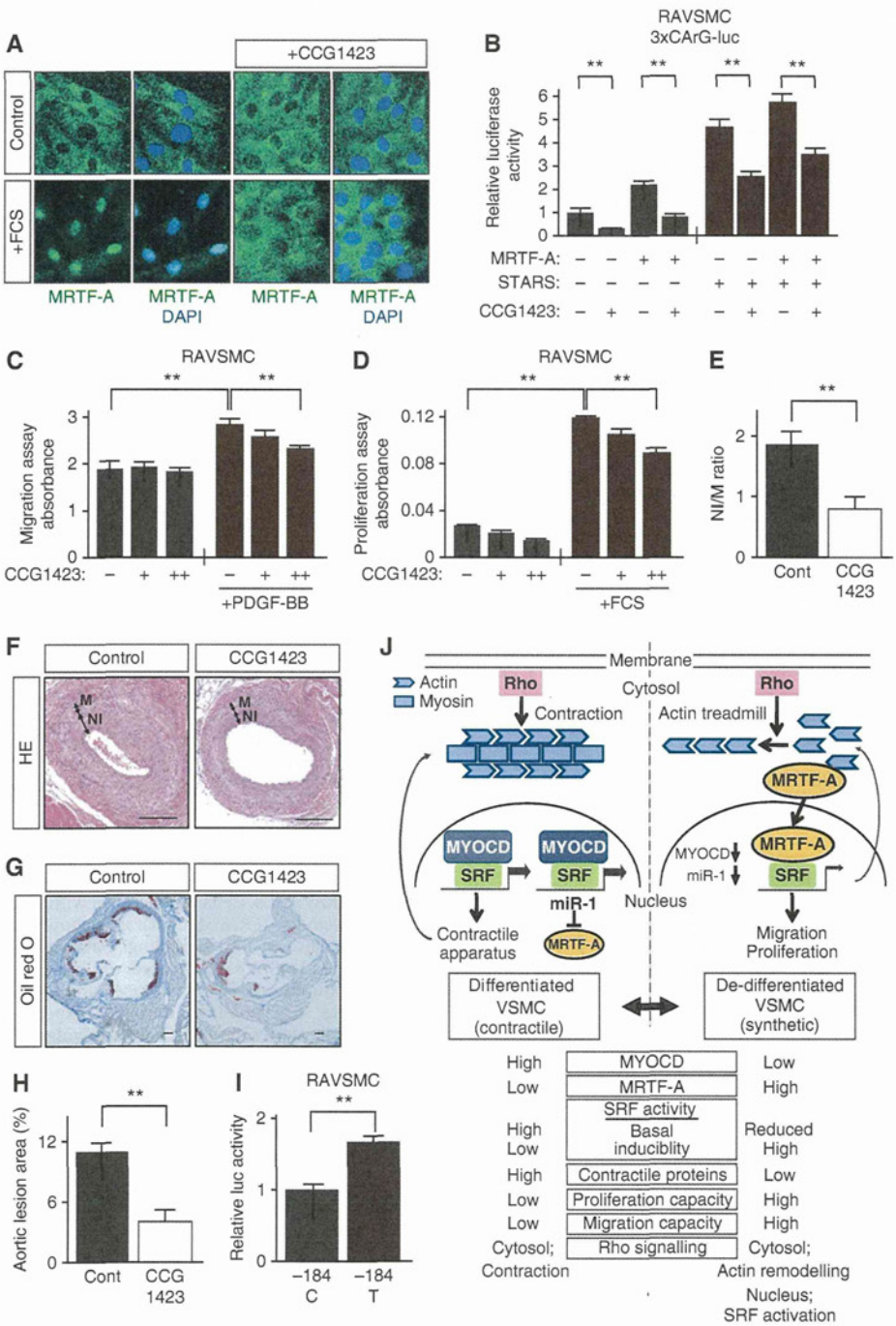

development of atherosclerotic lesions in *ApoE*$^{-/-}$ mice fed a high cholesterol diet for 6 weeks (Figure 6G and H; Supplementary Figure S6F).

Recently, it has been revealed that an SNP in the promoter region of the human MRTF-A gene (−184C>T), which results in a high transcriptional activity in HeLa and K562 cells, is associated with susceptibility to CAD (Hinohara *et al*, 2009). We found that the −930 bp of MRTF-A promoter containing −184T, which is associated with high CAD susceptibility, showed significantly stronger transcriptional activity than the wild-type promoter in cultured RAVSMCs (Figure 6I). These results further support our notion that inhibition of MRTF-A could be an effective novel approach to the treatment and prevention of vascular disorders.

Discussion

In the present study, we used three vascular injury models (femoral artery wire injury, carotid artery ligation and diet-induced atherosclerosis in *APOE*$^{-/-}$ mice) in *Mkl1*$^{-/-}$ mice to elucidate the roles played by MRTF-A in pathological vascular remodelling. We initially found that expression of MRTF-A mRNA and protein was significantly increased in injured arteries and aortic tissues containing atherosclerotic lesions in *ApoE*$^{-/-}$ mice, while expression of myocardin was reciprocally decreased. In each model, neointima formation or atherosclerotic lesions were significantly smaller in *Mkl1*$^{-/-}$ mice than in the respective controls. The expression of vinculin, MMP-9 and integrin β1 genes, which are targets of SRF and key regulators of cellular migration, was significantly diminished in the injured arteries of *Mkl1*$^{-/-}$ mice. Knocking down MRTF-A in RAVSMCs reduced expression of these genes in response to extracellular stimuli, which significantly impaired cell migration. These results demonstrate that induced expression of MRTF-A is crucial for acquisition of the capacity to migrate in response to environmental stress in dedifferentiated VSMCs (Liu *et al*, 2005). We also found that MRTF-A gene expression in VSMCs is, at least in part, regulated by miR-1, which is in turn regulated by myocardin and SRF (Jiang *et al*, 2010; Chen *et al*, 2011). Expression of miR-1 was reduced in dedifferentiated VSMCs, along with that of myocardin. This apparently led to an increase in MRTF-A expression, though it is possible that another as yet unidentified mechanism, such as transcriptional regulation through sites located in the distal 5′-FR or within introns, also contribute to the reciprocal regulation of myocardin and MRTF-A expression. Finally, we showed that a small molecule inhibitor of MRTF-A, CCG-1423, significantly reduced neointima formation following wire injury to mouse femoral arteries. Collectively, these results demonstrate that induction of MRTF-A plays a key role in vascular remodelling by maintaining SRF activity, thereby conferring a capacity for migration in response to extracellular stimuli on dedifferentiated VSMCs. MRTF-A is thus a potentially useful therapeutic target that may be more specific and efficient than the upstream Rho family GTPases, which can affect diverse intracellular signalling events.

In differentiated VSMCs, myocardin strongly activates SRF and the expression of VSMC-specific contractile proteins, thereby contributing to the maintenance of the contractile phenotype (Wang *et al*, 2003). Myocardin is constitutively located in the nucleus, where it suppresses MRTF-A expression via activation of miR-1. The ability of MRTF-B to transduce Rho signalling into the nucleus is much weaker than that of MRTF-A (Kuwahara *et al*, 2005; Nakamura *et al*, 2010),

Table II Luminal and neointimal area of femoral arteries 3weeks after vascular injury

	n	Lumen ($\times 10^3/\mu m^2$)	Intima ($\times 10^3/\mu m^2$)	Media ($\times 10^3/\mu m^2$)	IEL ($\times 10^3/\mu m^2$)	EEL ($\times 10^3/\mu m^2$)	Intima/Media ratio
Control injury	6	15.0 ± 3.0	39.9 ± 4.1	22.9 ± 2.1	55.0 ± 2.4	77.8 ± 3.7	1.85 ± 0.17
CCG1423 injury	8	22.3 ± 5.6	20.2 ± 4.8*	24.8 ± 1.6	43.0 ± 7.2	67.8 ± 2.8	0.81 ± 0.19*

The ratio of intima to media was calculated as the intimal area/medial area. Values are means ± s.e.m. IEL, internal elastic lamina; EEL, external elastic lamina. *$P<0.01$ versus control injured arteries.

Figure 6 CCG-1423, an MRTF-A inhibitor, attenuated neointima formation induced by wire injury in mouse femoral arteries. (**A**) CCG-1423 diminished the nuclear accumulation of endogenous MRTF-A induced by 20% FCS in RAVSMCs. Cells were stained with anti-MRTF-A antibody (green) and DAPI (blue). (**B**) CCG-1423 significantly inhibited MRTF-A-induced SRF activity in RAVSMCs. Graphs show the relative luciferase activities of 3 × CArG-luc. STARS: expression plasmid encoding striated muscle activator of Rho signalling. Data were obtained from two experiments performed in quintuplicate. (**C**) PDGF-BB-induced migration was assessed in RAVSMCs treated without or with 0.1 μm (+) or 1 μm (++) of CCG-1423. Data were obtained from two experiments performed in sextuplicate. (**D**) FCS-induced proliferation was assessed in RAVSMCs treated without or with 0.1 μm (+) or 1 μm (++) of CCG-1423. Data were obtained from two experiments performed in quadruplicate. (**E, F**) Effect of CCG-1423 on neointima formation in wire-injured femoral arteries in mice. Graph showing the neointima (NI)-to-media (M) ratio in wire-injured arteries from mice treated without (control) or with CCG-1423 ($n=3$ in control group and 4 in CCG1423 group) (**E**). Representative images of neointima are shown (**F**). (**G**) Representative images of atherosclerotic lesions in cross-sections of proximal aorta from *ApoE*$^{-/-}$ mice fed a high-cholesterol diet with or without CCG-1423 for 6 weeks. Oil-red O: Oil-red O staining. Bar indicates 100 μm. (**H**) Graphs showing the relative (%) area of atherosclerotic lesions in cross-sections of proximal aorta from *ApoE*$^{-/-}$ mice fed a high-cholesterol diet and treated with or without CCG-1423 for 6 weeks ($n=3$ in control group and 4 in CCG-1423 group). **$P<0.01$. (**I**) Effect of an SNP in the promoter region of MRTF-A gene (−184C>T) on the promoter activity in RAVSMCs. Relative activities of −930 bp MRTF-A(−184C)-luc and −930 bp MRTF-A(−184T)-luc in two different experiments performed in quadruplicate are shown. All graphs are shown as means ± s.e.m. **$P<0.01$. (**J**) A proposed model of the role of MRTF-A in vascular remodelling. In differentiated, contractile VSMCs, constitutively nuclear myocardin strongly activates SRF, leading to expression of VSMC-specific contractile proteins, and suppresses MRTF-A expression through activation of miR-1. Under these conditions, cytosolic Rho signalling is confined almost exclusively to regulation of contraction. In dedifferentiated VSMCs, MRTF-A expression is induced by reductions in miR-1 expression and basal SRF activity, thereby maintaining the lower basal SRF activity necessary for cellular migration and proliferation. Because MRTF-A is shuttled between the cytosol and nucleus and because it activates SRF downstream of Rho signalling, in dedifferentiated VSMCs, extracellular stimuli activating Rho signalling can substantively affect cellular proliferation and migration by modulating SRF activity. MYOCD: myocardin.

so that Rho family signalling is almost exclusively confined to regulating contraction through modifying Ca^{2+} sensitivity in the cytosol. By contrast, in dedifferentiated synthetic VSMCs, the reduction in myocardin expression leads to a reduction in basal SRF activity and then to a loss of VSMC-specific contractile components. Under these conditions, MRTF-A expression is induced, at least in part, by the reduction in miR-1 also caused by diminished myocardin, and is sufficient to maintain the SRF activity necessary for cellular migration and proliferation. Because MRTF-A is shuttled between the cytosol and nucleus, where it activates SRF downstream of Rho family GTPase-actin signalling, in dedifferentiated VSMCs extracellular stimuli activating Rho GTPase signalling can substantively affect cellular proliferation and migration by modulating SRF activity (Medjkane *et al*, 2009; Olson and Nordheim, 2010). Loss or inhibition of MRTF-A reduced stimulus-induced cell migration and proliferation, making cells static (Figure 6J). This suggests that the reciprocal expression of MRTF-A and myocardin mediated by miR-1 regulates the plasticity of effectors downstream of Rho family signalling, thereby contributing to phenotypic modulation of VSMC during vascular remodelling.

In addition to the classical concept that dedifferentiated intimal VSMCs are derived from medial VSMCs, recent evidence raises the possibility that VSMC progenitor cells in the circulation or adventitia also contribute to intimal VSMCs (Sata *et al*, 2002; Hoglund *et al*, 2010). We have not addressed the role of MRTF-A in the process of intimal VSMC differentiation from such progenitor cells in this study. In that context, however, MRTF-A has been shown to be involved in the differentiation of mesenchymal stem cells into VSMCs (Jeon *et al*, 2008). Thus, MRTF-A may also play an important role in the molecular processes underlying migration, proliferation and differentiation of VSMC progenitor cells into intimal VSMCs during vascular remodelling.

Recently, human genetic screening to identify novel susceptibility loci for CAD using microsatellite markers and SNP analysis revealed that an SNP in the promoter region of the MRTF-A gene ($-184C>T$) is associated with susceptibility to CAD (Hinohara *et al*, 2009). Moreover, functional analysis suggested that heightened MRTF-A expression is associated with increased susceptibility to CAD. We observed that the MRTF-A promoter containing $-184T$, which is associated with high CAD susceptibility, showed significantly stronger transcriptional activity than the wild-type promoter in cultured VSMCs (Figure 6I). These observations further support the conclusion that MRTF-A is crucially involved in pathological vascular remodelling underlying the development of vascular diseases, and imply that MRTF-A is a potentially useful therapeutic target for prevention of the progression of vascular diseases.

Materials and methods

Plasmids

-930 bp MRTF-A($-184C$)-luc (MRTF-A-luc), vinculin-luc, vinculin CArG-mut-luc and $3\times$CArG-luc were described previously (Kuwahara *et al*, 2007; Morita *et al*, 2007; Hinohara *et al*, 2009). Expression vectors used in the experiments were described previously (Kuwahara *et al*, 2007). MRTF-A 3′UTR-luc and mutMRTF-A 3′UTR-luc were respectively generated by inserting the MRTF-A 3′UTR containing wild type or mutated miR-1 target sequences downstream of the luciferase gene in a pMIR-REPORTER kit miRNA reporter expression vector (Ambion). -5500 bp MRTF-A-luc was generated by inserting 5500 bp of the 5′-FR of MRTF-A gene upstream of the luciferase gene in pGL4 vector (Promega).

Animal experiments

MRTF-A$^{-/-}$ mice were kindly provided from Dr EN Olson (The University of Texas, Southwestern Medical Center at Dallas) (Li *et al*, 2006). *ApoE*$^{-/-}$ and *MRTF-A*$^{-/-}$ mice (C57BL/6 background) were cross-bred (Kobayashi *et al*, 2004; Li *et al*, 2006). The animal care and all experimental protocols were reviewed and approved by the Animal Research Committee at Kyoto University Graduate School of Medicine.

Cell culture and transfection

RAVSMCs (Cell Applications. Inc.), A7r5 (DS Pharma Biomedical), NIH3T3 and COS7 cells were maintained in DMEM supplemented with 10% FCS. Co-transfection of RAVSMCs with $3\times$CArG-luc plus expression plasmids encoding MRTF-A (1 ng) and STARS (100 ng), or with MRTF-A-luc plus expression plasmids encoding myocardin and MRTF-A (0, 1 or 10 ng each) was accomplished using FuGene6 (Roche). pRL-TK (Roche) was included in all transfections as an internal control. MiRIDIAN microRNA mimic for miR-1, miRIDIAN microRNA hairpin inhibitor for miR-1 or a negative control for each (Thermo Scientific) was transfected into RAVSMCs grown in 6-cm dishes using Dharmafect2. MAVSMCs were obtained as previously reported (Nakamura *et al*, 2010).

RNA interference

RAVSMCs grown in 6-cm dishes were transfected with 200 pmol of ON-TARGET plus® siRNA reagent targeting rat MRTF-A or myocardin, or control scrambled siRNA (Thermo Scientific) using Dharmafect 2. For luciferase assays, RAVSMCs grown in 24-well dishes were transfected with 100 pmol of siRNA and 500 ng of luciferase reporter plasmid using Fugene 6.

Mouse vascular injury

Vascular wire injury was induced in femoral arteries of male C57BL/6 wild-type or *Mkl1*$^{-/-}$ mice at 8–10 weeks of age, as described previously (Sata *et al*, 2000; Takaoka *et al*, 2009). LNA oligonucleotide anti-miR-1 microRNA inhibitor or LNA microRNA inhibitor negative control (20 mg/kg) (5′-FAM prelabelled, Exiqon) was injected into sham-operated or injured femoral arteries from the muscular branch using a syringe with 29 gauge needle (TERUMO).

Quantification of neointimal hyperplasia

We harvested the femoral and carotid arteries 4 weeks after wire injury, unless otherwise indicated. Digitalized images were analysed using image analysis software (Image J, NIH), and the intimal and medial areas were recorded. The average of the neointima/media ratios in FIVE serial sections was designated as the value to represent each individual.

Analysis of atherosclerotic lesion area in ApoE$^{-/-}$ mice

Mkl1$^{+/-}$;*ApoE*$^{-/-}$ and *Mkl1A*$^{-/-}$;*ApoE*$^{-/-}$ mice were fed normal chow for 4 weeks beginning when the mice were 4 weeks old. Then beginning when they were 8 weeks old, they were fed a high-cholesterol diet (F2HFD1, Oriental Biotechnology) for 8 weeks. Atherosclerotic lesions were analysed by en-face analysis of the whole aorta and quantified by cross-sectional analysis of the proximal aorta, as described previously (Paigen *et al*, 1987; Palinski *et al*, 1994; Kobayashi *et al*, 2004).

Immunohistochemical analysis

Paraffin-embedded sections (4 μm thick) of femoral arteries harvested 4 weeks after wire injury were stained with anti-Mac3, anti-CD31, mouse monoclonal anti-αSMA (Sigma-Aldrich), rabbit polyclonal anti-SM-MHC (BT-562, Biomedical Technologies Inc.) or anti-BSAC antibodies (Sasazuki *et al*, 2002). Ratios of total numbers of Mac-3-positive cells in the intima and the media and CD31-positive endothelial cells in *Mkl1*$^{+/+}$ and *Mkl1*$^{-/-}$ mice were quantified ($n=4$ and 5 in each group, respectively). Sections of proximal aortas from *ApoE*$^{-/-}$ mice were stained with anti-α-SMA, anti-SM-MHC or anti-BSAC antibody.

Real-time RT–PCR

Real-time one-step RT–PCR was performed using One-step RT-PCR master mix reagent (Applied Biosystems). MiR-1 expression was determined using a Taqman MicroRNA RT kit and Taqman Universal PCR Master Mix II (Applied Biosystems). All taqman primers and probes were purchased from Applied Biosystems.

Western blot analysis

Western blot analysis was performed using rabbit polyclonal anti-myocardin, anti-MRTF-A and anti-MRTF-B antibodies as described previously (Kuwahara *et al*, 2005; Nakamura *et al*, 2010).

Statistical analysis

Data are presented as means ± s.e.m. Unpaired *t*-tests were used for comparison between two groups, and ANOVA with *post hoc* Fisher's test was used for comparison among groups. Values of $P<0.05$ were considered as significant. Data obtained from the two-way factorial design were analysed with the two-way ANOVA.

Supplementary data

Supplementary data are available at *The EMBO Journal* Online (http://www.embojournal.org).

Acknowledgements

We thank H Yanagisawa (The University of Texas Southwestern Medical Center at Dallas), T Murayama, H Arai, E Ashihara and T Maekawa (Kyoto University) for their technical instruction; Y Kubo for her excellent secretarial work; K Hinohara (Tokyo Medical and Dental University) for preparation of MRTF-A-luciferase constructs; and F Kataoka, A Fujishima and A Abe for their excellent technical assistance. We also gratefully thank EN Olson and R Bassel-Duby (The University of Texas Southwestern Medical Center at Dallas) for providing us MRTF-A knockout mice. This research was supported by Grants-in-Aid for Scientific Research from the Japan Society for the Promotion of Science (to KK, AK and K N); a grant from the Japanese Ministry of Health, Labour and Welfare (to KN); grants from the Japan Foundation for Applied Enzymology, the Mitsubishi Pharma Research Foundation, the Astellas Foundation for Research on Metabolic Disorders, the Vehicle Racing Commemorative Foundation, the Takeda Medical Research Foundation, the Takeda Science Foundation, the Hoh-ansha Foundation, the SENSHIN Medical Research Foundation (to KK) and the Kimura Memorial Heart Foundation (to HK).

Author Contributions: TM conducted most of the experiments and contributed to data analysis. KK and NK conceived of and directed the project. MT, HK, YK, MS, TS and RN provided technical help on animal experiments. YN, HN, TN, KS and AK performed some experiments using luciferase reporter assays, immunohistochemical analysis and western blot analysis with TM. KN, YY, CY, JS, SU, TN and YK contributed to data analysis.

Conflict of interest

The authors declare that they have no conflict of interest.

References

Bentzon JF, Weile C, Sondergaard CS, Hindkjaer J, Kassem M, Falk E (2006) Smooth muscle cells in atherosclerosis originate from the local vessel wall and not circulating progenitor cells in ApoE knockout mice. *Arterioscler Thromb Vasc Biol* **26:** 2696–2702

Chen J, Yin H, Jiang Y, Radhakrishnan SK, Huang ZP, Li J, Shi Z, Kilsdonk EP, Gui Y, Wang DZ, Zheng XL (2011) Induction of microRNA-1 by myocardin in smooth muscle cells inhibits cell proliferation. *Arterioscler Thromb Vasc Biol* **31:** 368–375

Daniel JM, Bielenberg W, Stieger P, Weinert S, Tillmanns H, Sedding DG (2010) Time-course analysis on the differentiation of bone marrow-derived progenitor cells into smooth muscle cells during neointima formation. *Arterioscler Thromb Vasc Biol* **30:** 1890–1896

Evelyn CR, Wade SM, Wang Q, Wu M, Iniguez-Lluhi JA, Merajver SD, Neubig RR (2007) CCG-1423: a small-molecule inhibitor of RhoA transcriptional signaling. *Mol Cancer Ther* **6:** 2249–2260

Glass CK, Witztum JL (2001) Atherosclerosis. The road ahead. *Cell* **104:** 503–516

Hinohara K, Nakajima T, Yasunami M, Houda S, Sasaoka T, Yamamoto K, Lee BS, Shibata H, Tanaka-Takahashi Y, Takahashi M, Arimura T, Sato A, Naruse T, Ban J, Inoko H, Yamada Y, Sawabe M, Park JE, Izumi T, Kimura A (2009) Megakaryoblastic leukemia factor-1 gene in the susceptibility to coronary artery disease. *Hum Genet* **126:** 539–547

Hinson JS, Medlin MD, Lockman K, Taylor JM, Mack CP (2007) Smooth muscle cell-specific transcription is regulated by nuclear localization of the myocardin-related transcription factors. *Am J Physiol Heart Circ Physiol* **292:** H1170–H1180

Hoglund VJ, Dong XR, Majesky MW (2010) Neointima formation: a local affair. *Arterioscler Thromb Vasc Biol* **30:** 1877–1879

Jeon ES, Park WS, Lee MJ, Kim YM, Han J, Kim JH (2008) A Rho kinase/myocardin-related transcription factor-A-dependent mechanism underlies the sphingosylphosphorylcholine-induced differentiation of mesenchymal stem cells into contractile smooth muscle cells. *Circ Res* **103:** 635–642

Jiang Y, Yin H, Zheng XL (2010) MicroRNA-1 inhibits myocardin-induced contractility of human vascular smooth muscle cells. *J Cell Physiol* **225:** 506–511

Jin W, Goldfine AB, Boes T, Henry RR, Ciaraldi TP, Kim EY, Emecan M, Fitzpatrick C, Sen A, Shah A, Mun E, Vokes V, Schroeder J, Tatro E, Jimenez-Chillaron J, Patti ME (2011) Increased SRF transcriptional activity in human and mouse skeletal muscle is a signature of insulin resistance. *J Clin Invest* **121:** 918–929

Kenagy RD, Hart CE, Stetler-Stevenson WG, Clowes AW (1997) Primate smooth muscle cell migration from aortic explants is mediated by endogenous platelet-derived growth factor and basic fibroblast growth factor acting through matrix metalloproteinases 2 and 9. *Circulation* **96:** 3555–3560

Kobayashi T, Tahara Y, Matsumoto M, Iguchi M, Sano H, Murayama T, Arai H, Oida H, Yurugi-Kobayashi T, Yamashita JK, Katagiri H, Majima M, Yokode M, Kita T, Narumiya S (2004) Roles of thromboxane A(2) and prostacyclin in the development of atherosclerosis in apoE-deficient mice. *J Clin Invest* **114:** 784–794

Kuwahara K, Barrientos T, Pipes GC, Li S, Olson EN (2005) Muscle-specific signaling mechanism that links actin dynamics to serum response factor. *Mol Cell Biol* **25:** 3173–3181

Kuwahara K, Teg Pipes GC, McAnally J, Richardson JA, Hill JA, Bassel-Duby R, Olson EN (2007) Modulation of adverse cardiac remodeling by STARS, a mediator of MEF2 signaling and SRF activity. *J Clin Invest* **117:** 1324–1334

Li S, Chang S, Qi X, Richardson JA, Olson EN (2006) Requirement of a myocardin-related transcription factor for development of mammary myoepithelial cells. *Mol Cell Biol* **26:** 5797–5808

Li S, Wang DZ, Wang Z, Richardson JA, Olson EN (2003) The serum response factor coactivator myocardin is required for vascular smooth muscle development. *Proc Natl Acad Sci USA* **100:** 9366–9370

Liu Y, Sinha S, McDonald OG, Shang Y, Hoofnagle MH, Owens GK (2005) Kruppel-like factor 4 abrogates myocardin-induced activation of smooth muscle gene expression. *J Biol Chem* **280:** 9719–9727

Medjkane S, Perez-Sanchez C, Gaggioli C, Sahai E, Treisman R (2009) Myocardin-related transcription factors and SRF are required for cytoskeletal dynamics and experimental metastasis. *Nat Cell Biol* **11:** 257–268

Miano JM (2003) Serum response factor: toggling between disparate programs of gene expression. *J Mol Cell Cardiol* **35:** 577–593

Miralles F, Posern G, Zaromytidou AI, Treisman R (2003) Actin dynamics control SRF activity by regulation of its coactivator MAL. *Cell* **113:** 329–342

Morita T, Mayanagi T, Sobue K (2007) Reorganization of the actin cytoskeleton via transcriptional regulation of cytoskeletal/focal adhesion genes by myocardin-related transcription factors (MRTFs/MAL/MKLs). *Exp Cell Res* **313:** 3432–3445

Nakamura S, Hayashi K, Iwasaki K, Fujioka T, Egusa H, Yatani H, Sobue K (2010) Nuclear import mechanism for myocardin family

members and their correlation with vascular smooth muscle cell phenotype. *J Biol Chem* **285:** 37314–37323

Nishimura G, Manabe I, Tsushima K, Fujiu K, Oishi Y, Imai Y, Maemura K, Miyagishi M, Higashi Y, Kondoh H, Nagai R (2006) DeltaEF1 mediates TGF-beta signaling in vascular smooth muscle cell differentiation. *Dev Cell* **11:** 93–104

Olson EN, Nordheim A (2010) Linking actin dynamics and gene transcription to drive cellular motile functions. *Nat Rev Mol Cell Biol* **11:** 353–365

Owens GK, Kumar MS, Wamhoff BR (2004) Molecular regulation of vascular smooth muscle cell differentiation in development and disease. *Physiol Rev* **84:** 767–801

Paigen B, Morrow A, Holmes PA, Mitchell D, Williams RA (1987) Quantitative assessment of atherosclerotic lesions in mice. *Atherosclerosis* **68:** 231–240

Palinski W, Ord VA, Plump AS, Breslow JL, Steinberg D, Witztum JL (1994) ApoE-deficient mice are a model of lipoprotein oxidation in atherogenesis. Demonstration of oxidation-specific epitopes in lesions and high titers of autoantibodies to malondialdehyde-lysine in serum. *Arterioscler Thromb* **14:** 605–616

Sasazuki T, Sawada T, Sakon S, Kitamura T, Kishi T, Okazaki T, Katano M, Tanaka M, Watanabe M, Yagita H, Okumura K, Nakano H (2002) Identification of a novel transcriptional activator, BSAC, by a functional cloning to inhibit tumor necrosis factor-induced cell death. *J Biol Chem* **277:** 28853–28860

Sata M, Maejima Y, Adachi F, Fukino K, Saiura A, Sugiura S, Aoyagi T, Imai Y, Kurihara H, Kimura K, Omata M, Makuuchi M, Hirata Y, Nagai R (2000) A mouse model of vascular injury that induces rapid onset of medial cell apoptosis followed by reproducible neointimal hyperplasia. *J Mol Cell Cardiol* **32:** 2097–2104

Sata M, Saiura A, Kunisato A, Tojo A, Okada S, Tokuhisa T, Hirai H, Makuuchi M, Hirata Y, Nagai R (2002) Hematopoietic stem cells differentiate into vascular cells that participate in the pathogenesis of atherosclerosis. *Nat Med* **8:** 403–409

Schwartz SM, deBlois D, O'Brien ER (1995) The intima. Soil for atherosclerosis and restenosis. *Circ Res* **77:** 445–465

Shoji M, Sata M, Fukuda D, Tanaka K, Sato T, Iso Y, Shibata M, Suzuki H, Koba S, Geshi E, Katagiri T (2004) Temporal and spatial characterization of cellular constituents during neointimal hyperplasia after vascular injury: Potential contribution of bone-marrow-derived progenitors to arterial remodeling. *Cardiovasc Pathol* **13:** 306–312

Sun Y, Boyd K, Xu W, Ma J, Jackson CW, Fu A, Shillingford JM, Robinson GW, Hennighausen L, Hitzler JK, Ma Z, Morris SW (2006) Acute myeloid leukemia-associated Mkl1 (Mrtf-a) is a key regulator of mammary gland function. *Mol Cell Biol* **26:** 5809–5826

Takaoka M, Nagata D, Kihara S, Shimomura I, Kimura Y, Tabata Y, Saito Y, Nagai R, Sata M (2009) Periadventitial adipose tissue plays a critical role in vascular remodeling. *Circ Res* **105:** 906–911

Wang D, Chang PS, Wang Z, Sutherland L, Richardson JA, Small E, Krieg PA, Olson EN (2001) Activation of cardiac gene expression by myocardin, a transcriptional cofactor for serum response factor. *Cell* **105:** 851–862

Wang DZ, Li S, Hockemeyer D, Sutherland L, Wang Z, Schratt G, Richardson JA, Nordheim A, Olson EN (2002) Potentiation of serum response factor activity by a family of myocardin-related transcription factors. *Proc Natl Acad Sci USA* **99:** 14855–14860

Wang Z, Wang DZ, Pipes GC, Olson EN (2003) Myocardin is a master regulator of smooth muscle gene expression. *Proc Natl Acad Sci USA* **100:** 7129–7134

Watanabe N, Kurabayashi M, Shimomura Y, Kawai-Kowase K, Hoshino Y, Manabe I, Watanabe M, Aikawa M, Kuro-o M, Suzuki T, Yazaki Y, Nagai R (1999) BTEB2, a Kruppel-like transcription factor, regulates expression of the SMemb/Nonmuscle myosin heavy chain B (SMemb/NMHC-B) gene. *Circ Res* **85:** 182–191

Xu W, Baribault H, Adamson ED (1998) Vinculin knockout results in heart and brain defects during embryonic development. *Development* **125:** 327–337

Zhao Y, Samal E, Srivastava D (2005) Serum response factor regulates a muscle-specific microRNA that targets Hand2 during cardiogenesis. *Nature* **436:** 214–220

Development/Plasticity/Repair

Glucocorticoid Suppresses Dendritic Spine Development Mediated by Down-Regulation of Caldesmon Expression

Daisuke Tanokashira,[1]* Tsuyoshi Morita,[1]* Ken'ichiro Hayashi,[1]* Taira Mayanagi,[1,3] Kentaro Fukumoto,[1,3,4] Yoshiko Kubota,[3] Toshihide Yamashita,[2] and Kenji Sobue[1,3]

Departments of [1]Neuroscience and [2]Molecular Neuroscience, Graduate School of Medicine, Osaka University, Suita, Osaka 565-0871, Japan, [3]Department of Neuroscience, Institute for Biomedical Sciences, Iwate Medical University, Yahaba-cho, Shiwa-gun, Iwate 028-3694, Japan, and [4]Department of Neuropsychiatry, School of Medicine, Iwate Medical University, Morioka, Iwate, 020-8505, Japan

Glucocorticoids (GCs) mediate the effects of stress to cause structural plasticity in brain regions such as the hippocampus, including simplification of dendrites and shrinkage of dendritic spines. However, the molecular mechanics linking stress and GCs to these effects remain largely unclear. Here, we demonstrated that corticosterone (CORT) reduces the expression levels of caldesmon (CaD), causing dendritic spines to become vulnerable. CaD regulates cell motility by modulating the actin-myosin system and actin filament stability. In cultured rat hippocampal neurons, CaD localized to dendritic spines by binding to filamentous actin (F-actin), and CaD expression levels increased during spine development. CaD stabilized the F-actin dynamics in spines, thereby enlarging the spine heads, whereas CaD knockdown decreased the spine-head size via destabilization of the F-actin dynamics. CaD was also required for chemical LTP-induced actin stabilization. The CaD expression levels were markedly decreased by exposure to CORT mediated by suppression of serum response factor-dependent transcription. High CORT levels reduced both the spine-head size and F-actin stability similarly to CaD knockdown, and overexpressing CaD abolished the detrimental effect of CORT on dendritic spine development. These results indicate that CaD enlarges the spine-head size by stabilizing F-actin dynamics, and that CaD is a critical target in the GC-induced detrimental effects on dendritic spine development.

Introduction

Glucocorticoid (GC) hormones are principal stress mediators released from the adrenal gland in response to stressful events. Prolonged stress and chronic GC exposure produce abnormal behaviors in experimental animals and an increased risk of psychiatric disorders in humans (McEwen, 1999, 2005; Phillips et al., 2005; Becker et al., 2007). In animals, maternal stress during pregnancy increases GC levels not only in the mother but also in the fetus, leading to structural alterations in the developing brain and abnormal behaviors in adult offspring (Weinstock, 2008). In humans, prenatal stress is associated with increased anxiety in adolescence and a greater incidence of psychiatric disorders in adulthood (McEwen, 2005; Phillips et al., 2005; Becker et al., 2007). Antenatal GC therapy in humans has been shown to reduce both the convolution index and surface area of the cortex (Modi et al., 2001). Exposure to repeated stress and excessive GCs adversely affects neuronal architecture, causing dendritic branches to atrophy and reducing the density of dendritic spines and changing spine morphology (Watanabe et al., 1992; Magariños et al., 1996; Wellman, 2001; Radley et al., 2004, 2006; Liston and Gan, 2011). Thus, repeated exposure to stress-induced GCs results in alterations of neuronal architecture related to psychiatric disorders, but the precise molecular and cellular mechanisms of these alterations have been largely unclear.

Most excitatory synapses are located in the dendritic spines, which are small actin-rich protrusions that change shape from filopodia to stubby or mushroom-shaped spines during the course of neuron development (von Bohlen Und Halbach, 2009). Spine morphology and density are of importance as structural foundation in cognitive function and behavior (Dumitriu et al., 2010; Bloss et al., 2011). Actin filaments, a central component of dendritic spines, regulate the spine morphology, dynamics, and function (Hotulainen and Hoogenraad, 2010). In long-term potentiation (LTP), which is considered a cellular event for memory formation, the spine heads enlarge and synaptic connections are strengthened. Actin filament formation is tightly associated with the establishment of LTP (Lisman, 2003; Hotulainen and Hoogenraad, 2010). Thus, actin dynamics play an important role in synaptic development and plasticity. Although chronic stress and GC exposure are reported to impair synaptic development and plasticity (Radley et al., 2006; Liston and Gan, 2011), the molecular mechanisms of their association with actin dynamics remain poorly understood.

Received May 16, 2012; revised Aug. 1, 2012; accepted Aug. 21, 2012.

Author contributions: T. Morita, K.H., T.Y., and K.S. designed research; D.T., T. Morita, K.H., T. Mayanagi, K.F., and Y.K. performed research; D.T., T. Morita, K.H., and T. Mayanagi analyzed data; T. Morita and K.S. wrote the paper.

This work was supported by Grants-in-aid for Scientific Research 20240038 from the Japan Society for the Promotion of Science (to K.S.) and 23110510 from the Ministry of Education, Culture, Sports, Science and Technology (MEXT) (to K.S).

*D. T., T. Morita, and K. H. contributed equally to this work.

The authors declare no competing financial interests.

Correspondence should be addressed to Dr. Kenji Sobue, Department of Neuroscience, Institute for Biomedical Sciences, Iwate Medical University, 2-1-1 Nishitokuta, Yahaba-cho, Shiwa-gun, Iwate 028-3694, Japan. E-mail: ksobue@iwate-med.ac.jp.

DOI:10.1523/JNEUROSCI.2380-12.2012

 0270-6474/12/3214583-09$15.00/0

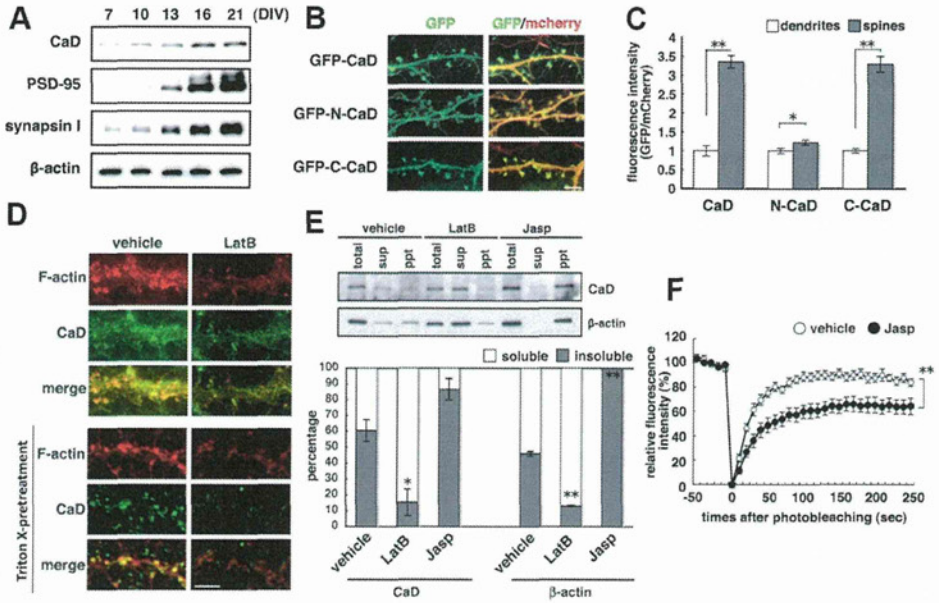

Figure 1. CaD expression profile and localization in developing hippocampal neurons. ***A***, CaD, PSD-95, and synapsin I protein expression profiles. ***B***, GFP-CaD, GFP-N-CaD, or GFP-C-CaD was exogenously expressed in neurons, using mCherry protein as a cell volume marker (scale bar, 5 μm). GFP and mCherry fluorescence intensities were measured in dendritic shafts and spines, respectively. ***C***, The graph shows GFP intensities corrected for mCherry intensities. CaD associates with F-actin (*$p < 0.05$, **$p < 0.01$). ***D***, Hippocampal neurons treated with DMSO (vehicle) or LatB for 3 h were incubated with (bottom) or without (top) 1% Triton X-100, then fixed and stained with anti-CaD antibody (green) and phalloidin (F-actin, red) (scale bar, 5 μm). ***E***, Neurons were treated with DMSO (vehicle), LatB, or Jasp, and then lysed with a solution containing Triton X-100. The lysates were separated into Triton X-soluble and -insoluble fractions by centrifugation. Western blotting was performed using equal load volumes of the fractions (top), and the CaD and β-actin proteins were quantified by densitometry (bottom). Data are means ± SE of values from three independent experiments (*$p < 0.05$, **$p < 0.01$). ***F***, GFP-CaD fluorescence recovery over time after photobleaching, measured in neurons treated with DMSO (vehicle) or jasplakinolide (Jasp). Data are means ± SE of values from 10 cells from three independent experiments (**$p < 0.01$).

Caldesmon (CaD) is a ubiquitous actin-linked regulatory protein that binds to and stabilizes actin filaments (Sobue and Sellers, 1991; Mayanagi and Sobue, 2011). GCs affect expression level of CaD, which negatively controls the radial migration of neural progenitor cells by regulating actin-myosin interactions, leading to transiently retarded neocortical development (Fukumoto et al., 2009). CaD also regulates axon extension by inhibiting myosin II function (Morita et al., 2012). Thus, the CaD-mediated regulation of actin dynamics is important for brain development. However, the role of CaD in spine development is unclear. In this study we demonstrated that CaD stabilizes actin filaments and increases the head size of dendritic spines in hippocampal neurons, while GCs decrease CaD expression levels and cause the detrimental effects on spine development.

Materials and Methods

Antibodies. This study used the following purchased antibodies: anti-PSD-95 (MA1-045, Affinity BioReagents), anti-β-actin (A5441, Sigma), anti-SRF (sc-335, Santa Cruz Biotechnology), anti-GAPDH (FL-335, Santa Cruz Biotechnology), anti-GFP (A11120 and A11122, Invitrogen), and anti-DsRed (632496, Clontech). Anti-CaD and anti-synapsin1 antibodies were produced in rabbits.

Cell culture. Since the medium generally used to culture hippocampal neurons includes a B27 supplement containing an undisclosed concentration of CORT, we used CORT-free B27 supplement commissioned from Invitrogen and added CORT to the medium to reach defined concentrations. Hippocampal neurons were prepared from rats on embryonic day 18.5. Dispersed neurons were plated on poly-L-lysine-coated coverslips and cultured in glial-conditioned MEM containing 1 mM sodium pyruvate, 0.6% (W/V) D-glucose, and either 2% standard B27 supplement (Invitrogen) or 2% CORT-free B27 supplement with the indicated concentrations of CORT added. After 1 week, one-half of the medium was changed to neurobasal (Invitrogen) medium containing 0.5 mM L-glutamine (Sigma) with either 2% standard B27 supplement or 2% CORT-free B27 supplement with the indicated concentrations of CORT added, and the neurons were cultured for another 2 weeks. All experiments using the cultured rat hippocampal neurons were performed during 21–24 d *in vitro* (DIV). All animal experiments were performed in accordance with guidelines from the Osaka University School of Medicine and the Iwate Medical University.

Foot-shock stress. Male Wistar rats (9–10 weeks old) (Japan SLC) were housed under controlled 12 h/12 h light/dark (lights on at 7:00 A.M.) and temperature (23 ± 2°C) conditions. Rats were randomly allocated to stress or control groups, and rats in the stress group were subjected to a single session of foot shocks. Foot-shock stress was applied in a foot-shock box with a grid floor connected to a shock generator (Med Associates) controlled by FreezeFrame software (Actimetrics). During this session, the rats received four uncontrollable, inescapable foot shocks (current intensity, 1.0 mA; duration, 1.0 s at random intervals of 60–90 s). After the session, the rat remained in the chamber for 60 s and was then returned to its home cage.

Determination of CORT concentrations. To avoid the influence of time-related CORT fluctuations, all experiments using live rats were performed between 10:30 A.M. and 11:00 A.M. Rats were anesthetized and decapitated, and blood was collected from the heart. The blood plasma was collected by centrifugation. At the same time, the brain was quickly removed, and cerebral tissue samples were individually homogenized in ice-cold PBS using a Potter–Elvehjem homogenizer and an ultrasound sonicator. Tissue homogenates were centrifuged and the supernatants were collected. Blood plasma and brain extracts were immediately stored at −80°C. CORT concentrations in these samples were determined with the Corticosterone EIA Kit (YK240, Yanaihara), which directly determines CORT concentrations using specially formulated sample diluents that displace CORT-binding globulin (CBG).

Expression plasmids and transfection. The coding regions for human *l*-CaD and its N terminus (1–263 aa) and C terminus (264–558 aa) and for human β-actin were amplified by PCR and subcloned into the highly efficient mammalian expression plasmid pCAGGS. EGFP, mCherry, or the myc-tag sequence was fused to the 5′ end of the coding sequences.

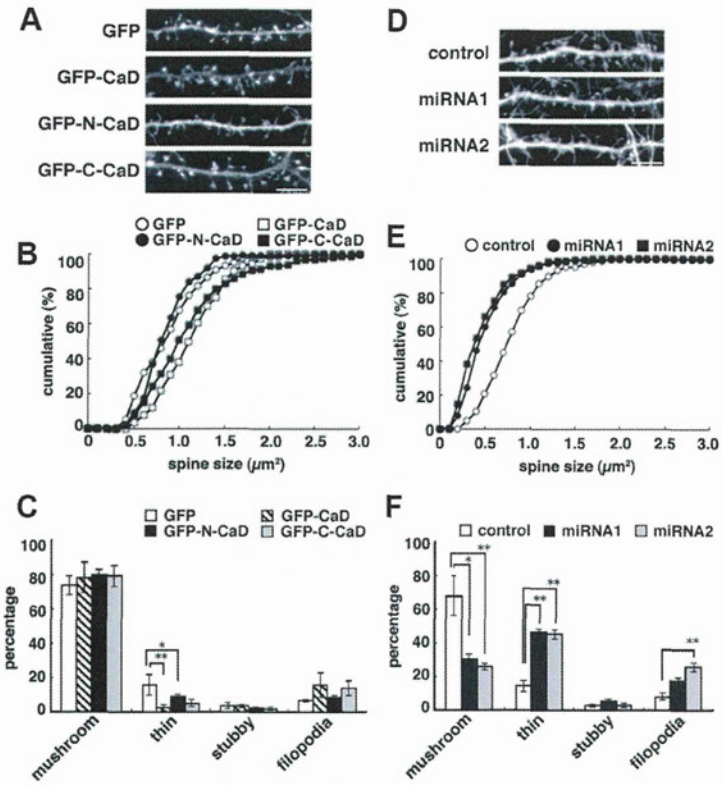

Figure 2. CaD regulates spine size in hippocampal neurons. ***A***, Spine morphology in neurons transfected with GFP, GFP-CaD, GFP-N-CaD, or GFP-C-CaD (scale bar, 10 μm), and graphs of spine sizes and their cumulative distributions (***B***), and classification of spine morphology (***C***). ***D***, Spine morphology in neurons transfected with control miRNA, CaD miRNA1, or CaD miRNA2 (scale bar, 10 μm), and graphs of spine sizes and their cumulative distributions (***E***), and classification of spine morphology (***F***).

The mCherry-LifeAct and miRNA plasmids were constructed as previously reported (target sequences: CaD miRNA1, GAGATGTATCTGGCAAGCGGA; CaD miRNA2, CTGGAGCAATATACCAATGCA) (Fukumoto et al., 2009; Morita et al., 2012). Hippocampal neurons were transfected by the calcium phosphate method as described previously (Jiang and Chen, 2006). Transfection was performed at 7 DIV (for miRNA) or 19 DIV (for CaD-overexpression).

Imaging. Neurons were cultured on coverslips, fixed using 4% paraformaldehyde, incubated with a primary antibody, and then incubated with the appropriate Alexa-labeled secondary antibody. To visualize filamentous actin (F-actin), Alexa 568-phalloidin (Invitrogen) was added in the secondary antibody solution. Stained neurons were observed under a BIOREVO BZ-9000 (Keyence) fluorescence microscope with an ×100 oil-immersion lens. Living neurons were cultured in a glass-bottom dish with Tyrode's solution (119 mM NaCl, 2.5 mM KCl, 25 mM HEPES, 30 mM glucose, 2 mM $CaCl_2$, and 2 mM $MgCl_2$, pH 7.4) and observed under an LSM5 PASCAL laser-scanning microscope (Carl Zeiss) with an ×63 oil-immersion lens.

To monitor actin turnover in dendritic spines, neurons transfected with GFP and mCherry-β-actin were analyzed by FRAP assay as previously described (Star et al., 2002). A high-intensity 543 nm He-Ne laser was used to bleach the mCherry fluorescence in single spines, and the fluorescence recovery was observed with a low-power laser every 10 s. GFP fluorescence was simultaneously detected with a 488 nm argon laser to monitor spine volume change. Actin turnover in the spine was evaluated by the fluorescence recovery of mCherry-β-actin, corrected for background and GFP intensity to avoid the influence of spine volume changes during observation. The GFP-CaD dynamics in spines were also analyzed by FRAP. Neurons were transfected with GFP-CaD and mCherry. The GFP-CaD fluorescence in a single spine was bleached and the fluorescence recovery was observed every 10 s. The GFP-CaD intensity was corrected for background and mCherry intensity. The FRAP curve was fit to the equation: $F(t) = 1 - f_s - f_f * \exp^{(-t/\lambda)}$ in the previous report (Star et al., 2002), where f_s, f_f, t, and λ are the stable fraction, dynamic fraction, time (second), and time constant, respectively. The time constant during fluorescence recovery was analyzed according to the equation for the first 60 s.

To monitor F-actin dynamics in dendritic spines, neurons were transfected with GFP and mCherry-LifeAct. Fluorescence was detected every 10 s. F-actin dynamics were evaluated by the average change rate per 10 s of mCherry intensity, corrected for background and EGFP intensity to avoid the influence of spine volume change during observation. Actin-depolymerizing drug, latrunculin B (LatB, 5 μM), and actin-stabilizing drug jasplakinolide (Jasp, 100 nM) were used in actin dynamics-targeted experiments.

Chemical LTP. Chemical LTP (cLTP) was induced in cultured hippocampal neurons as previously described (Otmakhov et al., 2004). Neurons were incubated for 15 min in Tyrode's solution containing 6 μM 2-chloroadenosine. The solution was replaced by $MgCl_2$-free Tyrode's solution containing 100 μM picrotoxin, 50 μM forskolin, and 0.1 μM rolipram, and the neurons were incubated for another 15 min. After cLTP was induced, the solution was washed out with normal Tyrode's solution. Neurons were observed 3 h after cLTP induction.

Triton X-100-insoluble cytoskeletons. Neurons were treated with BRB buffer (10 mM PIPES pH 7.4, 3 mM NaCl, 100 mM KCl, 3.5 mM $MgCl_2$, and 1.25 mM EGTA) containing 1% Triton X-100 and protease inhibitor cocktail (Takara) for 2 min and were then washed with Triton X-100-free BRB buffer. The neurons were fixed and stained with anti-CaD antibody and phalloidin. For sedimentation assays, neurons were lysed with BRB buffer containing Triton X-100, and the lysate was separated by ultracentrifugation at 100,000 × g for 2 h. The supernatant and pellet were subjected to Western blotting as the Triton X-soluble and -insoluble fractions, respectively.

Quantitative real-time PCR. Total RNA was extracted from neurons, and cDNA was synthesized using the High-Capacity cDNA Reverse Transcription Kit (Applied Biosystems); mRNA levels were quantified by real-time PCR (RT-PCR) using SYBR GreenER qPCR SuperMix (Invitrogen) and were normalized to GAPDH mRNA expression. The respective primers were designed and synthesized by Sigma as follows: Gapdh-F (forward): CTCCCATTCTTCCACCTTTGATG, Gapdh-R (reverse): CCACCACCCTGTTGCTGTAG; Cald1-F: ATGTGGGAGAAAGGGAGTGTG, Cald1-R: CTTGGGAGCGGGTGACTTG, Cald1-Fibro-type-F: CTTGCTGGGTTGCTTAAAGG, Cald1-HeLa-type-F: CAGCTGCGGACATGCTTAG, Cald1-common-R: CTGTCACCTGTCCCAAGGAT; β-actin-F: CGTTGACATCCGTAAAGACCTC, β-actin-R: ATAGAGCCACCAATCCACACAG; PSD-95-F: CAGTGAGACCGACGACATTGG, PSD-95-R: ATGATGATGGGACGAGCATAGTG.

Reporter assays. The reporter constructs for the fibroblast-type promoter region of the rat *CALD1* gene were described previously (Fukumoto et al., 2009). The cells were lysed with Passive Lysis buffer (Promega), and the luciferase and β-galactosidase activities were measured using the luciferase assay system (Promega) and luminescent β-galactosidase detection kit II (Clontech), respectively.

Data quantification and statistics. Data from Western analysis were quantified by densitometry using ImageJ software. Data from synapse imaging were quantified using MetaMorph (Molecular Devices), BZ-II analysis application (Keyence; for fixed-cell imaging) or LSM5 PASCAL (Carl Zeiss; for live-cell imaging). All experiments were performed at